10 Della Torre E, Bozzolo EP, Passerini G, *et al*. IgG4-related pachymeningitis: evidence of intrathecal IgG4 on cerebrospinal fluid analysis. *Ann Intern Med* 2012; 156:401–3.
11 Vaglio A, Strehl JD, Manger B, *et al*. IgG4 immune response in Churg-Strauss syndrome. *Ann Rheum Dis* 2012;71:390–3.
12 Mujagic S, Sarihodzic S, Huseinagic H, *et al*. Wegener's granulomatosis of the paranasal sinuses with orbital and central nervous system involvement-diagnostic imaging. *Acta Neurol Belg* 2011;111:241–4.
13 Takuma H, Shimada H, Inoue Y, *et al*. Hypertrophic pachymeningitis with anti-neutrophil cytoplasmic antibody (p-ANCA), and diabetes insipidus. *Acta Neurol Scand* 2001;104:397–401.
14 Horino T, Takao T, Taniguchi Y, *et al*. Hypertrophic pachymeningitis with MPO-ANCA-positive vasculitis. *Clin Rheumatol* 2010;29:111–13.
15 Peng W, Wang X. Hypertrophic pachymeningitis and cerebral infarction resulting from ANCA-associated vasculitis. *Neurol India* 2012;60:424–6.
16 Berger JR, Snodgrass S, Glaser J, *et al*. Multifocal fibrosclerosis with hypertrophic intracranial pachymeningitis. *Neurology* 1989;39:1345–9.
17 Comings DE, Skubi KB, Van Eyes J, *et al*. Familial multifocal fibrosclerosis. Findings suggesting that retroperitoneal fibrosis, mediastinal fibrosis, sclerosing cholangitis, Riedel's thyroiditis, and pseudotumor of the orbit may be different manifestations of a single disease. *Ann Intern Med* 1967;66:884–92.
18 Yamamoto M, Takahashi H, Ohara M, *et al*. A new conceptualization for Mikulicz's disease as an IgG4-related plasmacytic disease. *Mod Rheumatol* 2006; 16:335–40.
19 Kamisawa T, Nakajima H, Egawa N, *et al*. IgG4-related sclerosing disease incorporating sclerosing pancreatitis, cholangitis, sialadenitis and retroperitoneal fibrosis with lymphadenopathy. *Pancreatology* 2006;6:132–7.
20 Kitano A, Shimomura T, Okada A, *et al*. Multifocal fibrosclerosis with intracranial pachymeningitis. *Intern Med* 1995;34:267–71.
21 Kim EH, Kim SH, Cho JM, *et al*. Immunoglobulin G4-related hypertrophic pachymeningitis involving cerebral parenchyma. *J Neurosurg* 2011; 115:1242–7.
22 Suzuki Y, Takeda Y, Sato D, *et al*. Clinicoepidemiological manifestations of RPGN and ANCA-associated vasculitides: an 11-year retrospective hospital-based study in Japan. *Mod Rheumatol* 2010;20:54–62.
23 Fujimoto S, Watts RA, Kobayashi S, *et al*. Comparison of the epidemiology of anti-neutrophil cytoplasmic antibody-associated vasculitis between Japan and the U. K. *Rheumatology (Oxford)* 2011;50:1916–20.
24 Zen Y, Nakanuma Y. IgG4-related disease: a cross-sectional study of 114 cases. *Am J Surg Pathol* 2010;34:1812–19.
25 Isobe N, Kira J, Kawamura N, *et al*. Neural damage associated with atopic diathesis: a nationwide survey in Japan. *Neurology* 2009;73:790–7.

Riku et al. Acta Neuropathologica Communications 2013, 1:12
http://www.actaneurocomms.org/content/1/1/12

ACTA NEUROPATHOLOGICA COMMUNICATIONS

CASE REPORT Open Access

Extensive aggregation of α-synuclein and tau in juvenile-onset neuroaxonal dystrophy: an autopsied individual with a novel mutation in the *PLA2G6* gene-splicing site

Yuichi Riku[1,2], Takeshi Ikeuchi[3], Hiroyo Yoshino[4], Maya Mimuro[5], Kazuo Mano[1], Yoji Goto[1], Nobutaka Hattori[6], Gen Sobue[1] and Mari Yoshida[5*]

Abstract

Background: Infantile neuroaxonal dystrophy (INAD) is a rare autosomal-recessive neurodegenerative disorder. Patients with INAD usually show neurological symptoms with infant onset and die in childhood. Recently, it was reported that mutations in the *PLA2G6* gene cause INAD, but neuropathological analysis of genetically confirmed individuals with neuroaxonal dystrophy has been limited.

Results: Here, we report a Japanese individual with neuroaxonal dystrophy associated with compound heterozygous mutations in the *PLA2G6* gene. A novel splice-site mutation resulting in skipping and missense mutations (p.R538C) in exon 9 was identified in the patient. This patient initially presented with cerebellar ataxia at the age of 3 years, which was followed by symptoms of mental retardation, extrapyramidal signs, and epileptic seizure. The patient survived until 20 years of age. Neuropathological findings were characterized by numerous axonal spheroids, brain iron deposition, cerebellar neuronal loss, phosphorylated alpha-synuclein-positive Lewy bodies (LBs), and phosphorylated-tau-positive neurofibrillary tangles. In particular, LB pathology exhibited a unique distribution with extremely severe cortical involvement.

Conclusions: Our results support a genetic clinical view that compound heterozygous mutations with potential residual protein function are associated with a relatively mild phenotype. Moreover, the severe LB pathology suggests that dysfunction of the *PLA2G6* gene primarily contributes to LB formation.

Keywords: α-synuclein, Infantile neuroaxonal dystrophy, Atypical neuroaxonal dystrophy, PLA2G6 gene, Tau

Background

Neurodegeneration with brain iron accumulation (NBIA) describes a group of progressive neurodegenerative disorders that are pathologically characterized by the presence of axonal spheroids and iron deposition in the brain [1-3]. These neurodegenerative diseases consist of a clinically and genetically heterogeneous group of disorders, including pantothenate kinase-associated neurodegeneration (PKAN, formerly known as Hallervorden-Spatz disease), infantile neuroaxonal dystrophy (INAD), and an unknown gene mutation-linked idiopathic neuroaxonal dystrophy [1,2,4]. PKAN is caused by mutations in the pantothenate kinase 2 (*PANK2*) gene, which accounts for the majority of NBIA patients [2]. Recently, it was reported that mutations in the phospholipase A2 group VI (*PLA2G6*) gene cause INAD [5], which is a rare autosomal-recessive neurodegenerative disorder. Patients with INAD usually present with psychomotor regression, truncal hypotonia, progressive ataxia, extrapyramidal symptoms, fast waves on an electroencephalogram, and neuro-ophthalmological abnormalities (e.g., optic atrophy, nystagmus, and strabismus) with infant onset and die in childhood [1,4,6]. However, in rare cases, patients with NAD caused by *PLA2G6* mutations present with heterogeneous neurological manifestations with onset past infanthood and survive until

* Correspondence: myoshida@aichi-med-u.ac.jp
[5]Institute for Medical Science of Aging, Aichi Medical University, Aichi, Japan
Full list of author information is available at the end of the article

adulthood with a slower disease progression [1,7,8]. In addition, mutations of the *PLA2G6* gene cause early onset dystonia-parkinsonism (PARK-14), which is clinically distinguished from NAD by good L-dopa responsiveness, L-dopa–induced dyskinesia, and dementia. These characteristics have been typically observed in patients with an older age of onset and with a longer disease duration compared to NAD, with no evidence of cerebellar symptoms [9]. Thus, these clinical phenotypes are collectively termed as *PLA2G6*-associated neurodegeneration [9].

We report a Japanese individual with neuroaxonal dystrophy that was associated with a novel compound heterozygous mutation in a splicing site of the *PLA2G6* gene. The clinical phenotype of this patient was atypical for INAD, occurred during late disease onset, and prolonged the disease course. Histopathological data revealed the presence of neuroaxonal spheroids, brain iron depositions, and cerebellar degeneration. Moreover, numerous Lewy bodies (LBs) and neurofibrillary tangles (NFTs), which are pathological hallmarks of Parkinson's disease (PD) and Alzheimer's disease (AD), respectively, were observed. Until recently, neuropathological analysis of genetically confirmed neuroaxonal dystrophy has been strongly limited due to a small number of patients [1,8]. In this study, we describe the clinicopathological characteristics of the patient and discuss the neuropathological implication of LBs and NFTs compared with PD and AD.

Case presentation

Clinical history

The patient was a Japanese man who died at 20 years of age. He exhibited normal development until the age of 3 years, at which time his parents noted his slurred speech and unstable gait. There was no evidence of a consanguineous marriage in any of his relatives. His grand-aunt had been diagnosed with "parkinsonism", and she died at the age of 60; however, her clinical diagnosis was uncertain. At the age of six, the patient was referred to our hospital due to a progressive gait disturbance and dysarthria. A neurological examination revealed cerebellar ataxia, bradykinesia, mental retardation, and hyperreflexia in the lower limbs without pathological reflexes. Truncal hypotonia and abnormalities in eye movement were not observed. Cerebral computed tomography (CT) showed severe cerebellar atrophy. The patient was clinically diagnosed with juvenile spinocerebellar degeneration, and taltirelin was administered for his ataxia; however, it did not have an effect. At the age of 12, cerebral magnetic resonance imaging (MRI) revealed severe atrophy of the cerebellum and mild atrophy of the frontal lobes (Figure 1a-c). The patient gradually became bedridden until the age of 15 and started experiencing repetitive generalized seizures. He was mainly treated with sodium valproate and phenobarbital. At the age of 18, he was re-admitted to our hospital, although he was nearly bedridden and could barely sit in a wheelchair at that time. Neurological examination revealed severe dystonia and rigidity in his limbs and neck, a masked face, and severe cerebellar ataxia. His tendon reflexes showed hyperreflexia in the upper limbs and were abolished in his lower limbs. Moreover, his plantar responses were flexor. CT and MRI (Figure 1d-f) revealed severe cerebellar and fronto-temporal lobe atrophy. The cerebral atrophy was more progressive compared to the atrophy observed when he was 12 years old. By T2-weighted imaging (T2WI), the bilateral globus pallidus (GP) and putamen exhibited low signal intensity. Tc99m-ECD-single-photon emission computed tomography revealed hypoperfusion in the fronto-temporal lobes and cerebellum (Figure 1g). An electroencephalogram showed multifocal spikes and theta waves in the right hemisphere in the absence of fast waves. The results of the nerve conduction study on the four limbs were normal. After discharge, a higher dose of valproate reduced the frequency of the patient's seizures; however, his rigidity and dystonia showed no response to L-DOPA treatment. The patient died of aspiration pneumonia.

Materials and methods

Neuropathological analysis

The postmortem interval was 5 hours. The brain and spinal cord were fixed in 20% neutral formalin. Samples obtained from the main representative regions of the brain and spinal cord were embedded in paraffin, sectioned into 4.5-μm-thick slides, and stained with hematoxylin and eosin (H&E), Klüver-Barrera staining, Prussian blue methods, and Gallyas-Braak (GB) staining. Immunohistochemical studies were performed on 4.5-μm-thick sections using an ENVISION kit (Dako) with diaminobenzidine (DAB; Wako, Osaka, Japan) as a chromogen. The primary antibodies used were anti-phosphorylated alpha-synuclein (p-α-synuclein) (pSyn#64, monoclonal mouse, 1:1000; Wako Pure Chemical Industries, Osaka, Japan), anti-ubiquitin (polyclonal rabbit, 1:2000; Dako), anti-amyloid-beta peptide (6F/3D, monoclonal mouse, 1:200; Dako), phosphorylated tau (p-tau) (AT8, monoclonal mouse, 1:2000; Innogenetics, Zwijndrecht, Belgium), anti- TDP-43 (TARDBP, polyclonal rabbit, 1:2500; ProteinTech, IL, USA), and anti-phosphorylated neurofilament (p-NF) (2F11, monoclonal mouse, 1:600; Dako). For double-immunofluorescence labeling, brain tissues obtained from the amygdala, oculomotor nucleus, and substantia nigra were sectioned into 4.5-μm-thick slides. The primary antibodies were anti-p-α-synuclein antibody and AT8 antibody. The secondary antibodies were goat anti-mouse IgG coupled with either

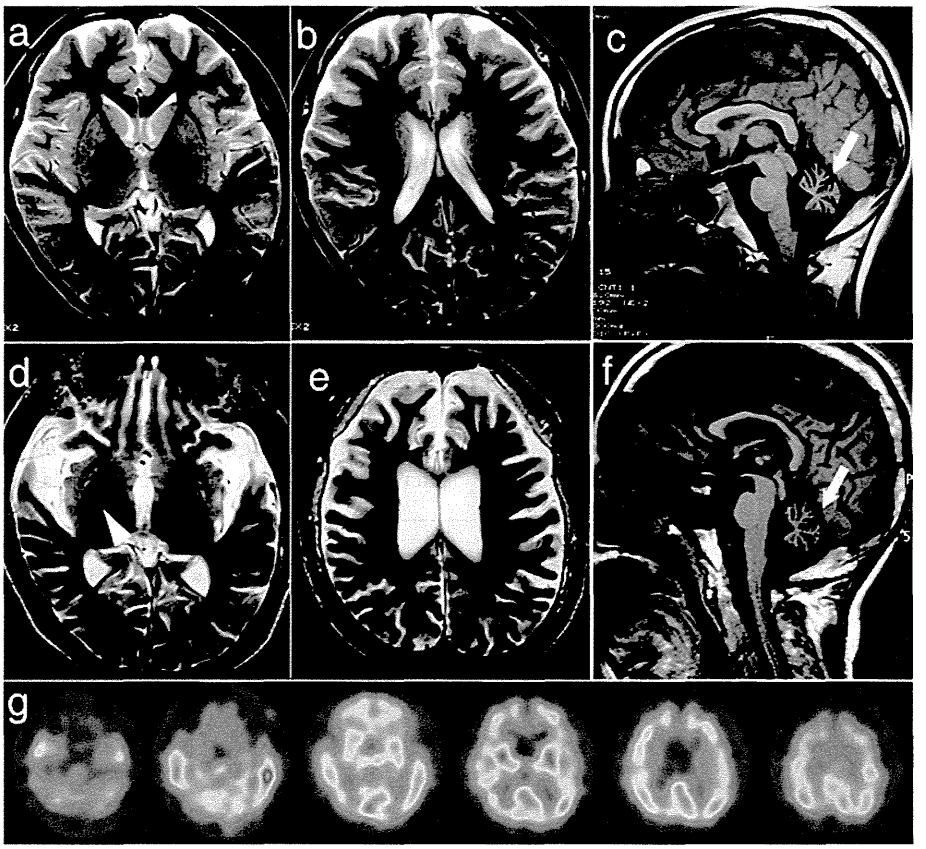

Figure 1 Magnetic resonance imaging (MRI) and Tc99m-ECD-single-photon emission computed tomography (SPECT) of the patient. **a-c** MRI at age 12. There was mild atrophy of the frontal cortex and slightly low intensity in the globus pallidus on T2-weighted images (T2WI) (**a, b**). The saggital section of the T1WI exhibited cerebellar atrophy (arrow) (**c**). **d-f** MRI at age 18. Low signal intensity in the globus pallidus (arrowhead) and atrophy of the temporal lobes was clear on the T2WI (**d**). The frontal lobes showed severe atrophy (**e**). The saggital section of the T1WI exhibited severe cerebellar atrophy (arrow) and thinness of the corpus callosum (**f**). An ECD-SPECT, at age 18, revealed hypoperfusion of the frontotemporal lobes and cerebellum (**g**).

Alexa Fluor 568 (1:300, emission peak 603 nm, Molecular Probes, OR, USA) or Alexa Fluor 488 (1:300, emission peak 517 nm, Molecular Probes). The slides were examined via confocal microscopy at × 200 and × 400 magnification using a Zeiss LSM 710 laser scanning confocal microscope.

For electron microscopy, sections from the cingulate gyrus were fixed in 4% glutaraldehyde. The sections were washed in phosphate buffer, postfixed with osmium tetroxide, dehydrated in a graded series of ethanol, and embedded in Epon. Ultrathin sections were stained with uranyl acetate and lead citrate.

Western blotting analysis of α-synuclein

Proteins expressed in the amygdala and parahippocampal gyrus of the autopsied patient and three control subjects were extracted as previously described [10,11]. Briefly, we fractionated the samples by resolubilization in increasingly stringent buffers (Tris-buffered saline, 1% Triton X-100, 1% sarcosyl, 8 M urea) as previously described. Equal amounts of supernatant protein were subjected to sodium dodecyl sulfate-polyacrylamide gel electrophoresis and immunoblotting. The mouse monoclonal antibody LB509 (Zymed Laboratories, South San Francisco, California) was used to detect α-synuclein. The monoclonal antibody pSyn#64 (Wako, Japan) specifically recognizes phosphorylated α-synuclein at serine 129 [12].

Genetic analysis

Genomic DNA was extracted from the frozen liver tissue of the patient using a standard procedure. Mutational analysis was performed using sequences of both strands of all of the PCR-amplified coding exons and the flanking intronic sequences of *PLA2G6, PANK-2, SNCA, parkin, PINK-1,* and *DJ-1.* Expansion of the CAG repeats of the SCA1, SCA3, DRPLA, and Huntington's disease genes was also examined. Genetic analysis of *PLA2G6* was also performed in the patient's parents. Total RNA was isolated from frozen brain tissue of the patient, and cDNA was synthesized using a High-Capacity cDNA

Reverse Transcription kit (Applied Biosystems). RT-PCR was performed using primer pairs to amplify the coding regions of the *PLA2G6* gene spanning exons 8–13 (5′-caacgtggagatgatcaagg-3′ and 5-gtcagcatcaccttgggttt-3′) and exons 9–13 (5′-ggaaggcgatcttgactctg-3′ and 5′-gtcagcatcaccttgggttt-3′). The institutional review board approved this study.

Results

Neuropathological findings

The patient's height was 150 cm, and his body weight was 39 kg. The brain weighed 890 g before fixation. Grossly, the cerebral hemispheres showed severe atrophy, particularly in the fronto-temporal cortex. In the brain sections, the most striking pathological finding was a light yellow-brown discoloration of the substantia nigra (SN), periaqueductal gray matter, putamen, caudate head, and GP (Figure 2a,b). The cerebellum was greatly reduced in size; its overall convolution pattern was retained, but the individual folia were shrunken.

Histopathologically, severe neuronal loss and gliosis were observed in the cerebral cortex, brainstem gray matter, and cerebellar cortex. In the cerebrum, neuronal loss was marked in the cingulate gyrus, fronto-temporal cortex, insular cortex, amygdala, and hippocampus. In the brain stem, neurons in the SN were markedly depleted, and the remaining neurons had low melanin content. The locus ceruleus (LC) showed moderate neuronal loss, but the neurons in the dorsal motor nucleus of the vagus were relatively spared. The cerebellar cortex showed severe neuronal loss (Figure 2c,d), particularly in the granule cell (gc) layer, and the parallel

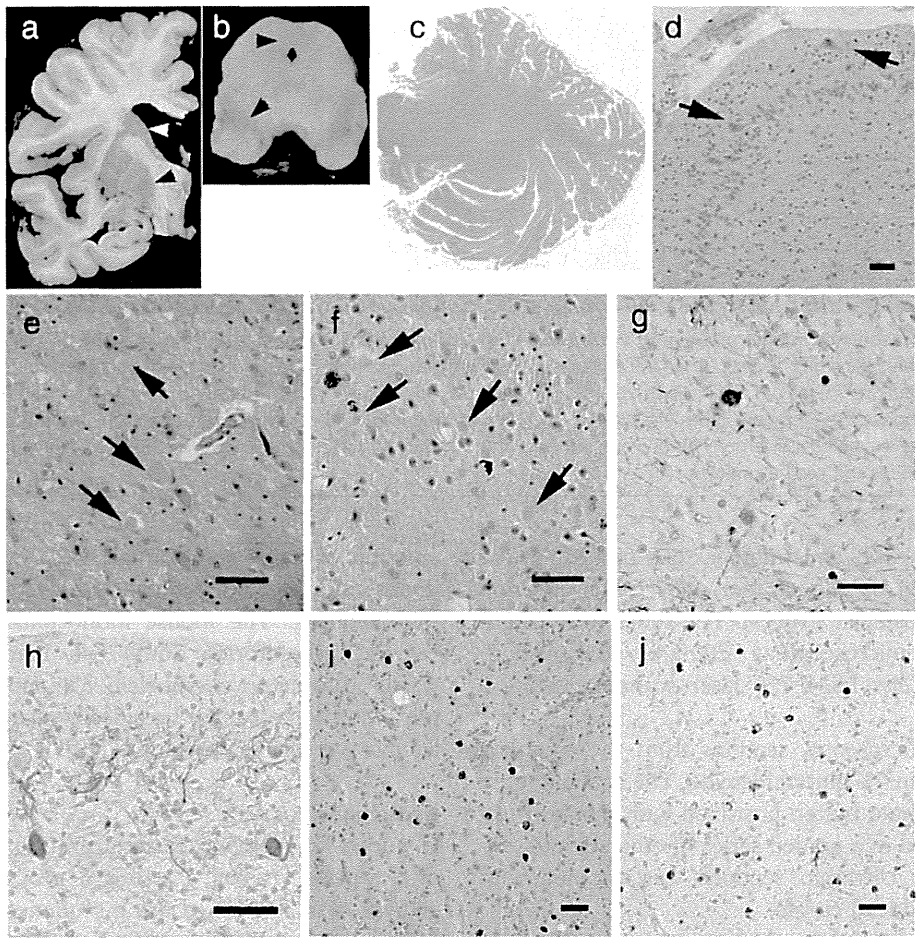

Figure 2 The macroscopic and microscopic findings in the patient. a, b The globus pallidus, putamen, caudate, substantia nigra, and periaqueductal gray matter demonstrated yellow-brown discoloration (arrowheads). **c** Grossly, the cerebellar cortex showed severe atrophy, and the granule cell layer was not visible. **d** The cerebellar granule cells were markedly depleted, and ectopic Purkinje cells (Pcs) were found (arrows). **e** The cingulate gyrus showed gliosis and numerous axonal spheroids (arrows). **f, g** The putamen also contained numerous axonal spheroids that were labeled by anti-phosphorylated neurofilament antibody. **h** In the cerebellum, anti-phosphorylated neurofilament immunostaining revealed dystrophic axons of the Pcs and highly reduced parallel fibers. **i** Many iron-positive granules were observed in the putaminal neuropil. **j** These granules were evident after Prussian blue staining. Bar = 50 μm. Hematoxylin and eosin staining (**c-f, i**), phosphorylated neurofilament immunohistochemistry (**g, h**), and Prussian-blue staining (**j**).

fibers in the molecular layer were strongly reduced (Figure 2c,d,h). Purkinje cells (Pcs) were severely depleted and often ectopically scattered at random in the molecular layer (Figure 2d). The spinal cord exhibited myelin pallor of the gracile fasciculus with gliosis.

In addition, we observed axonal spheroids throughout the central nervous system (CNS), particularly in the cerebral cortex, putamen (Figure 2e-g), caudate nucleus, nucleus accumbens, hypothalamus, SN, gracile nucleus, and spinal cord. The cerebellum contained numerous dystrophic axons called 'torpedoes' in the Pc and gc layers (Figure 2h). The diameters of the spheroids ranged from 10 to 20 μm, but the spinal cord contained larger-sized spheroids of 40–70 μm in diameter. Various spheroids were immunoreactive against anti-p-NF (Figure 2g,h) and anti-ubiquitin antibodies. We found no spheroids in the sympathetic ganglia, dorsal root ganglia, spinal roots, peripheral nerve fibers in the skin, or the enteric plexus. Brown-pigmented, Prussian blue-positive iron granules were scattered around the vessels and throughout the neuropil in the putamen, internal segment of the GP, caudate nucleus, thalamus, pars compacta of the SN, and periaqueductal gray matter (Figures 2i,j, 4c).

Furthermore, severe LB pathology was observed throughout the brain (Figures 3a-f, 4a). In immunohistochemistry, anti-p-α-synuclein (Figure 3c-f), anti-p-NF, and anti-ubiquitin antibodies strongly labeled LBs. Immunohistochemistry using anti-p-α-synuclein antibody also revealed numerous dilated and sausage-like dystrophic neurites in the neuropil, which have been referred to as Lewy neurites (LNs) (Figure 3d,e). In the

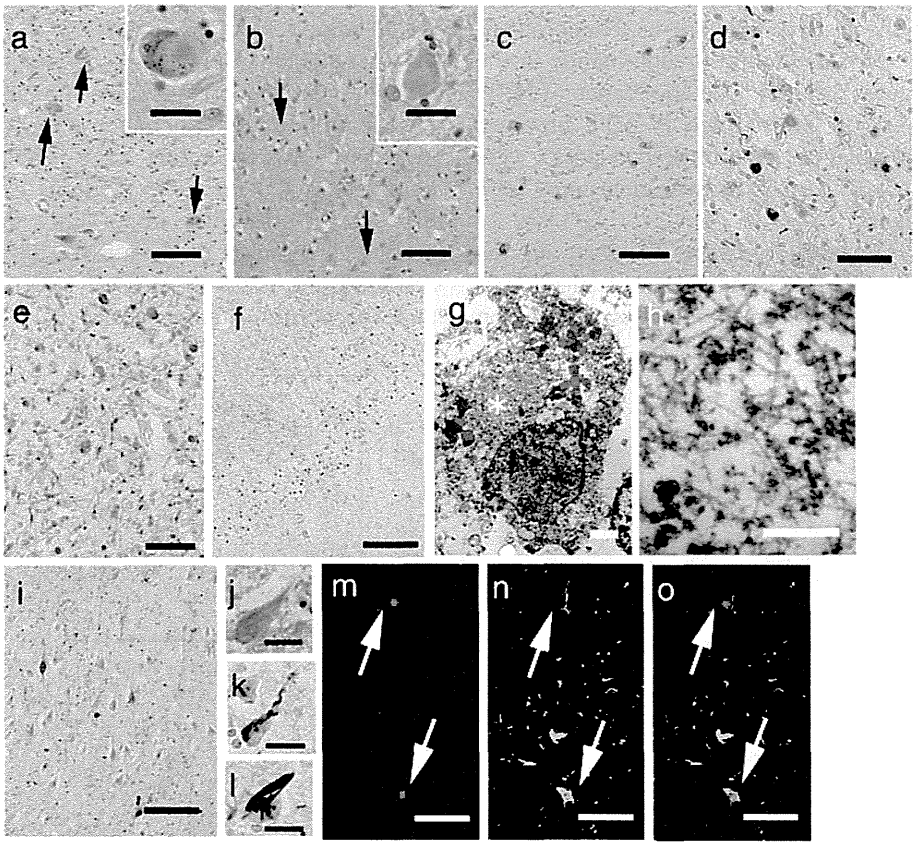

Figure 3 Lewy body (LB) and neurofibrillary tangle (NFT) pathology of the patient. a and inset The substantia nigra contained "brainstem-type" LBs with core and halo (arrows) structures. **b and inset** In the cingulate gyrus, the neuropil showed spongy changes in the deep layer, and there were "cortical-type" LBs without core and halo structures (arrows). **c and d** Anti-phosphorylated alpha-synuclein (p-α-synuclein) immunohistochemistry showed abundant LBs in the substantia nigra (**c**) and cingulate gyrus (**d**). **e and f** In the hypothalamus (**e**) and Ammon' s horn (**f**), p-α-synuclein-positive LBs and LNs were strikingly abundant. **g and h** Electron microscopy of a neuron in the cingulate gyrus showed cortical LBs in a cortical neuron (asterisk), which consisted of granular and filamentous structures. The filaments were arranged at random without a clear central zone density. **i - l** The pyramidal neuron in the hippocampal cortex contained abundant NFTs and threads that were positive for AT-8 antibody using the Gallyas-Braak method. **m-o** Confocal microscopy of the amygdala revealed immunoreactivity against p-α-synuclein (**m**, red), which often co-labeled with AT8 (**n**, green) in the same neurons (**o**, merged). Bar (**a**), (**b**), (**c**), and (**i**) = 100 μm; (**d**), (**e**), (**m**), (**n**), and (**o**) = 50 μm; (**f**) = 250 μm; (**g**) = 2 μm; (**h**) = 0.2 μm; (**a-inset**), (**b-inset**), (**j**), (**k**), and (**l**) = 20 μm. Hematoxylin and eosin staining (**a, b, j**), p-α-synuclein immunohistochemistry (**c-f**), AT8 immunohistochemistry (**i, k**), and Gallyas-Braak staining (**l**).

cerebral cortices, numerous cortical-type LBs, which lacked core and halo structures, and LNs were diffusely found (Figure 3b,e) with striking spongiform alterations (Figure 3b). The distribution and density of LBs and LNs exceeded what has been observed in advanced PD or DLB in the neocortical stage [13,14]. They were most abundant in the cingulate gyrus, amygdala, anterior hippocampus, CA2 region of the posterior hippocampus, and hypothalamus. LBs with a core and halo (brainstem-type LBs) were observed predominantly in the nucleus basalis of Meynert, SN, oculomotor nucleus, and LC (Figure 3a,c). In the cerebellum, neuronal cytoplasm and neurites of the dentate nucleus rarely contained p-α -synuclein-positive structures. In contrast, the olfactory bulbs and dorsal motor nucleus of the vagus contained only mild LB pathology. There were no p-α-synuclein-positive structures in the peripheral sympathetic ganglia, dorsal root ganglia, cardiac sympathetic nerve fibers, or nerve plexuses in the gastroenteric organs. Numerous p-tau-positive NFTs were also found predominantly in the limbic system (Figures 3i-l, 4b). The abundance of NFTs corresponded to AD in Braak stage IV [15], however, Aβ-positive neuritic plaques and amyloid deposits were absent. Additionally, TDP-43-positive inclusions were absent in this patient.

Using double-immunofluorescence labeling in the amygdala, p-tau-positive NFTs and p-α-synuclein-positive cortical LBs often co-labeled in the same neuron (Figure 3m-o). In contrast, neurons in the midbrain did not show co-labeling of LBs and NFTs (data not shown).

On electron microscopy, LBs from the cingulate gyrus consisted of closely packed 6- to 10-nm-thick granular and filamentous structures. The filaments were arranged at random without a clear central zone density. These findings were similar those observed in cortical-type LBs in the DLB [16] (Figure 3g,h).

Western blotting analysis of α-synuclein

To biochemically characterize the accumulation of α-synuclein, we sequentially extracted proteins from the amygdala and parahippocampal gyrus of the autopsied male subject using buffers with increasing capacities to solubilize proteins. In the control sample, immunoblotting analysis using anti-α-synuclein LB509 showed an approximately 15-kDa band corresponding to monomeric α-synuclein in Tris–HCl- and Triton X-100-soluble fractions (Figure 5a). In contrast, an ~15-kDa α-synuclein band was predominantly visualized in sarkosyl-insoluble urea-soluble fractions in the brain (Figure 5a). In addition to the ~15-kDa band, an ~30-kDa band corresponding to α-synuclein dimers was observed in the insoluble fractions extracted from the patient's brain samples. Importantly, the ~15- and ~30-kDa bands found in the urea-extracted fractions were reactive to anti-pSyn#64 antibody (Figure 5b), indicating that the accumulated α-synuclein in the patient brain

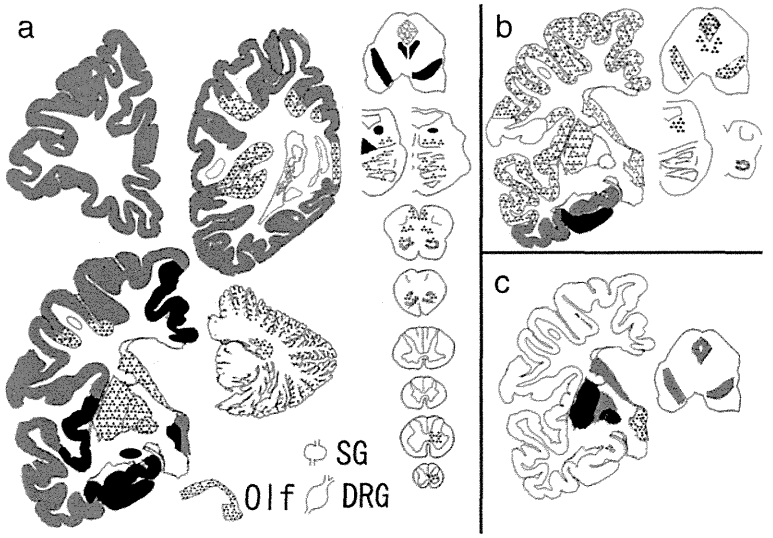

Figure 4 Schema of the distribution of Lewy bodies (LBs), neurofibrillary tangles (NFTs), and iron deposition in the patient. a LBs were diffusely spread in the cerebral cortices and were most abundant in the limbic system, hypothalamus, nucleus basalis of Meynert, substantia nigra (SN), and locus ceruleus. The olfactory bulbs and dorsal motor nucleus of the vagus contained only mild LB pathology. There were no p-α -synuclein-positive structures in the peripheral sympathetic ganglia and dorsal root ganglia. **b** NFTs were predominantly observed in the limbic system, which corresponded to Alzheimer's disease in Braak stage IV. **c** Iron-positive granules were found in the putamen, internal segment of the globus pallidus, caudate nucleus, SN, and periaqueductal gray matter. *DRG*: dorsal root ganglia, *Olf*: olfactory bulb, *SG*: sympathetic ganglia. Semi-quantitative scale for LBs and NFTs: *dot-pattern* = 1–10, *gray* = 10–20, *black* > 20. Number of lesions in a field observed using a 10× objective. Iron-positive granules: *dot-pattern* = mild, *gray* = moderate, *black* = severe.

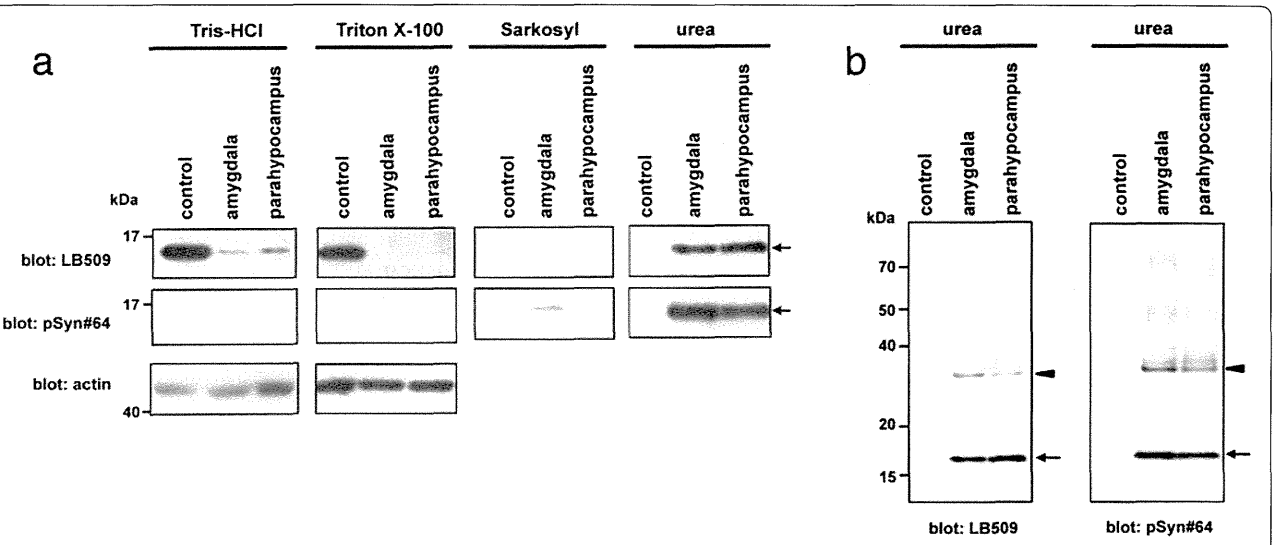

Figure 5 Biochemical analysis of α-synuclein in brain tissues. a The samples were sequentially fractionated by resolubilization with increasingly stringent buffers containing Tris-buffered saline, Triton X-100, sarkosyl, and urea. The samples were analyzed using the α-synuclein antibodies LB509 and pSyn#64. In the urea-extracted fraction, a phosphorylated α-synuclein band at approximately at ~15 kDa (arrow) was substantially accumulated in the brain (amygdala and parahippocampus) of the autopsied patient. Conversely, the level of α-synuclein in the Tris- and Triton X-100-soluble fractions was decreased. Anti-β-actin immunoblotting served as a loading control (bottom panel). **b** α-Synuclein-reactive fragments of dimers migrating at approximately ~30 kDa (arrowhead) and a smear at higher molecular weights were abundant in the urea-extracted fraction of the patient's brain.

was phosphorylated at serine 129. Moreover, the patient showed large amounts of α-synuclein-reactive high-molecular-weight smears, which might have represented α-synuclein oligomers (Figure 5b).

Genetic analysis

Sequence analysis revealed that the patient carried compound heterozygous mutations in the *PLA2G6* gene. A novel splice-site mutation in exon 9 (c.1187-2A > G) and a missense mutation (c.1612C > T, p.R538C) in exon 12 (Figure 6a) were identified in the patient. These mutations were absent in 120 normal control subjects. The p.R538C missense mutation was previously reported in patients with classical INAD [5]. Genetic analysis of the unaffected parents of the patient revealed that the father and mother were heterozygous carriers of the p.R538C missense and splice-site mutations, respectively (Figure 6b). No mutations were identified in *PANK2, SNCA, parkin, DJ-1, or PINK-1*. There was no pathological expansion of CAG repeats in the genes associated with SCA1, SCA2, DRPLA, or Huntington's disease.

We next investigated whether the splice-site mutation caused an alteration in the splicing of *PLA2G6* using RT-PCR analysis of total RNA extracted from the patient's frozen tissue. To examine the mRNA expression of *PLA2G6* in the patient's brain, two primer pairs were designed to amplify cDNA fragments encompassing exons 8 to 13 (primers A-C) and 9 to 13 (primers B-C), respectively (Figure 6c). In the control samples, two alternative splicing variants were amplified using the primer pairs A-C. Sequence analysis of the fragments in the control samples revealed that these variants corresponded to two previously reported isoforms of *PLA2G6* mRNA, with and without the 162-bp exon 9, respectively [17]. In the patient, the 700-bp fragment containing exon 9 was nearly undetectable by RT-PCR using the primer pair A-C. RT-PCR amplification using the primer pair B-C revealed that the 600-bp cDNA fragment containing exon 9 found in the control samples was less expressed in the patient (Figure 6d).

Discussion

INAD is a rare, autosomal-recessive neurodegenerative disorder with infant onset, and patients usually die in childhood [1,4,6]. In an INAD cohort with *PLA2G6* mutations previously described by Gregory et al., symptoms began between 5 months and 2.5 years of age [1]. Wu et al. reported that half of INAD patients with a disease course of 2–5 years became vegetative [6]. In this study, the patient's initial neurological manifestation was cerebellar ataxia at the age of 3 years, which was later accompanied by mental retardation, dystonia, and seizures. The patient survived until the age of 20 years. His clinical phenotype was atypical for INAD; the disease onset and progression were delayed and slower, and there was no indication of truncal hypotonia, neuro-ophthalmologic abnormalities, or fast rhythms on an electroencephalogram throughout the clinical course.

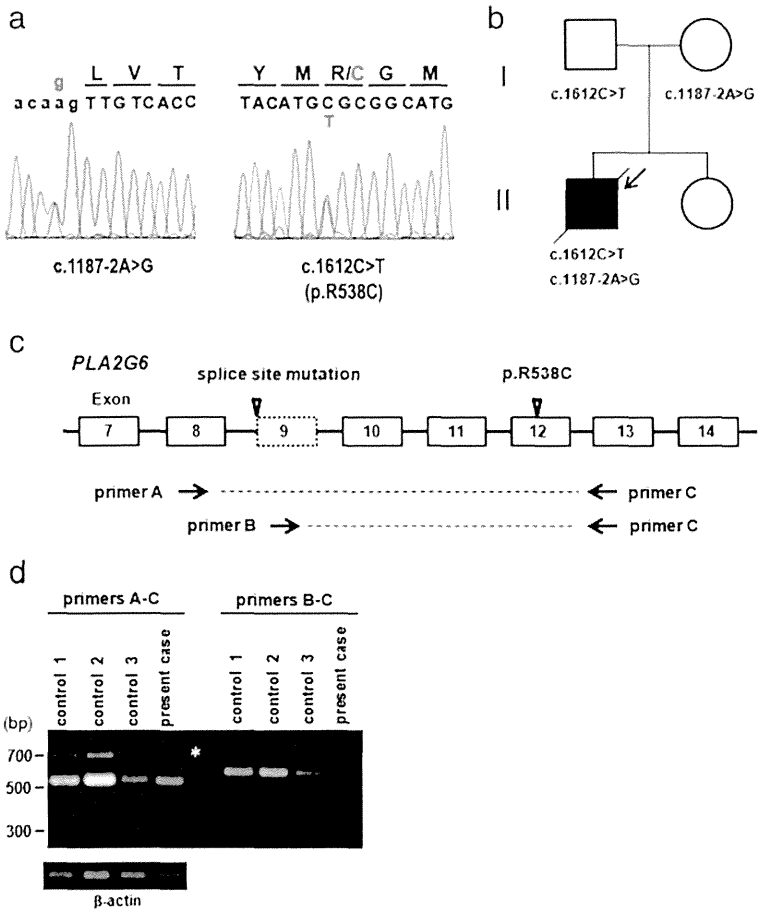

Figure 6 Identification of compound heterozygous mutations in *PLA2G6* in the patient. a Mutation analysis of *PLA2G6* in the patient. Sequence analysis of the patient's genomic DNA revealed two mutations: a 5′ splice-site mutation in exon 9 (c.1187-2A > G) and a missense mutation (c.1612C > T, p.R538C) in exon 12. The capital and small letters represent nucleotides in exons and introns, respectively. **b** Pedigree of the patient with *PLA2G6* mutations. Circle, female; square, male; slash through symbol, deceased individual; closed symbol, affected individual. An arrow denotes the proband. The father and mother each carried one of the compound heterozygous mutations found in the patient. **c** Schematic illustration of exon-intron structure of *PLA2G6*. Boxes represent exons. The positions of the mutations in the patient are shown. Two primer pairs were designed to amplify cDNA fragments encompassing exons 8 to 13 (primers A-C) and 9 to 13 (primers B-C). **d** Reverse transcription (RT)-PCR analysis of the patient's brain. In the patient, a 700-bp fragment containing exon 9 was nearly undetectable by RT-PCR using the primer pair A-C. RT-PCR amplification using the primer pair B-C revealed a 600-bp cDNA fragment containing exon 9, which was recognized in control samples but was less noticeable in the autopsied patient. Amplification of β-actin mRNA was used as an internal control.

Gregory et al. previously described six patients in their patient registry with *PLA2G6* mutation who exhibited variable clinical phenotypes with late onset (average 4.4 years, range 1.5-6.5 years) [1,2]. This phenotype was referred to as atypical neuroaxonal dystrophy (ANAD). The clinical phenotype of our patient might be classified as ANAD. Moreover, patients with a slower disease progression and heterogeneous clinical pictures have been occasionally described in other series of INAD patients [7,8]. Currently, it is speculated that patients with mutant forms of the *PLA2G6* gene display a complete absence of protein, which is associated with a severe INAD profile, whereas patients with compound heterozygous mutations potentially exhibit residual protein function and have a less severe phenotype [18]. Our genetic findings further support this genotype-phenotype correlation.

To the best of our knowledge, there have only been two reports that describe the CNS neuropathology of genetically confirmed patients with a *PLA2G6* gene mutation, as summarized in Table 1 [1,8]. The neuropathological features, including neuroaxonal spheroids, cerebellar degeneration, and brain iron accumulation, were described in INAD before the discovery of its causal gene [3]. Moreover, the presence of LB and NFT pathology has been described in neuroaxonal dystrophy with *PLA2G6* gene mutation [1,8]. On the basis of disease onset, patients 1–4 in Table 1 might be classified as ANAD or early onset dystonia-parkinsonism; however, no components of the pathological findings differed

Table 1 Summary of the neuropathological findings in autopsied patients with *PLA2G6* gene mutations in the literature

Patient	Age at onset	Age at death	Spheroids in the CNS	Spheroids in the PNS	Neuronal loss in the cerebellum	Accumulation of alpha synuclein	Accumulation of tau	Brain iron
1[8]	18 y	36 y	+	NA	gc and Pc	+	+	+
2[1]	3 y	23 y	+	-	gc and Pc	+	+	+
3[8]	childhood	18 y	+	NA	gc and Pc	+	+	+
4[8]	14 m	8 y	+	NA	gc and Pc	+	+	+
5[8]	infant	8 y	+	NA	NA	+	-	NA
Our patient	3 y	20 y	+	-	gc and Pc	+	+	+

Abbreviation: CNS = central nervous system; gc = granule cell; NA = not assessed; Pc = Purkinje cell; PNS = peripheral nervous system.

between these clinical phenotypes. In the current patient, neuronal loss, LB pathology, NFT pathology, and the presence of axonal spheroids were marked in the limbic system, fronto-temporal lobes, and SN. These pathological findings might be responsible for progressive cortical atrophy, psychomotor regression, and parkinsonism. Iron deposition broadly extended throughout the basal ganglia and midbrain compared to what was predicted from the T2 low-intensity area on MRI. Furthermore, loss of cerebellar neurons, particularly granule cells, was both striking and consistent with the cerebellar ataxia that was diagnosed in the early phase of the disease.

LB pathology has been identified in all six patients reviewed [1,8]. A recent study reported that LB pathology was not observed in patients with the *PANK2* gene mutation [19]. Moreover, earlier case reports describing neuroaxonal dystrophy or brain iron accumulation with abundant LBs may have been describing patients with *PLA2G6* gene mutations [20-22]. We demonstrated that the morphological, ultrastructural, and biochemical properties of LBs in this patient were identical to those in PD and diffuse Lewy body disease (DLB) patients [12,16,23]. Furthermore, the spatial distribution of LB pathology showed cortical involvement that exceeded that of the end stage of sporadic PD or the diffuse neocortical type of DLB [13,14]. Previous autopsy reports of INAD and ANAD have also described marked cortical involvement of LBs [1,8]. In contrast, the dorsal nucleus of the vagus nerve and olfactory bulbs were mildly affected in our patient, and the cardiac nerve fibers and enteral nerve plexus contained no p-α-synuclein aggregation, although these regions have been described as constant and early affected regions in sporadic PD and DLB [24,25]. The distribution of LB pathology in INAD and ANAD may tend to be more severe in the cerebral cortices compared to the medulla oblongata or peripheral autonomic neurons, which differs from the typical topography observed in sporadic PD and DLB. NFT pathology was another neuropathologial characteristic of interest in patients with INAD and ANAD. In our patient, NFTs and p-tau-positive threads predominantly appeared in the limbic system, which was similar to AD in Braak's stage IV [15]. However, neither this nor previously reported patients with *PLA2G6* gene mutations exhibited senile plaques, which contrasts with the typical neuropathology observed in AD [15]. Importantly, NFT pathology has been frequently observed in patients with sporadic PD or DLB [26,27], and LBs and NFTs often coexist in the same neurons, particularly those located in the limbic areas [26]. Our double-immunofluorescence results are consistent with findings in sporadic PD and DLB. Thus, further investigation in multiple patients on the association between NFTs and LB pathology and the implications of NFT pathology in INAD and ANAD are required.

The *PLA2G6* gene encodes iPLA2-Via, which is a critical protein in lipid membrane homeostasis [28]. Recent reports using Pla2g6-knockout mice demonstrated the presence of axonal spheroids in which tubulovesicular membranes accumulated [29-32]. In contrast, the pathological mechanism that contributes to LB formation in INAD and ANAD remains to be elucidated. LBs are secondarily present in several situations other than sporadic PD/DLB (e.g., sporadic or familial AD or Niemann-Pick disease type C) or may be incidentally found in healthy elderly individuals [33-36]. However, our neuropathological results and previous studies have demonstrated that LB pathology in patients with *PLA2G6* gene mutations shows a high prevalence and displays an extremely severe phenotype, particularly in the cerebral cortices. These findings suggest that defects in PLA2G6 primarily contribute to the formation of LBs.

Conclusions

Our results demonstrate the clinical heterogeneity of neuroaxonal dystrophy with *PLA2G6* gene mutations and support a genetic clinical view that compound heterozygous mutations that potentially result in residual protein function are associated with a less severe

phenotype. Neuropathologically, CNS involvement with LBs was striking and exhibited a unique topography compared with PD. Thus, further investigations on the process of LB formation caused by loss of *PLA2G6* gene function may provide new insights into the pathological mechanism of neuroaxonal dystrophy and LB formation.

Consent

Written informed consent was obtained from the patient's parents for publication of this Case report and any accompanying images. A copy of the written consent is available for review by the Editor-in chief of this journal.

Competing interests

There are no competing interests in the report.

Authors' contributions

YR, MM, and MY performed clinical and pathological analysis. TI, HY, and HH carried out the biochemical and genetic studies and drafted the manuscript. GS, KM, and YG helped to draft the manuscript. All authors read and approved the final manuscript.

Acknowledgement

This work was supported by Grants-in-Aid from the Research Committee of CNS Degenerative Diseases, the Ministry of Health, Labour and Welfare of Japan. The study was approved by the ethics committee of Juntendo University and Niigata University, and all subjects gave informed consent.

Author details

[1]Department of Neurology, Nagoya Daiichi Red Cross Hospital, Aichi, Japan. [2]Department of Neurology, Nagoya University Graduate School of Medicine, Aichi, Japan. [3]Department of Neurology, Brain Research Institute, Niigata University, Niigata, Japan. [4]Research Institute for Diseases of Old Age, Graduate School of Medicine, Juntendo University, Tokyo, Japan. [5]Institute for Medical Science of Aging, Aichi Medical University, Aichi, Japan. [6]Department of Neurology, Graduate School of Medicine, Juntendo University, Tokyo, Japan.

Received: 9 February 2013 Accepted: 5 April 2013
Published: 9 May 2013

References

1. Gregory A, Westaway SK, Holm IE, Kotzbauer PT, Hogarth P, Sonek S, Coryell JC, Nguyen TM, Nardocci N, Zorzi G, Rodriguez D, Desguerre I, Bertini E, Simonati A, Levinson B, Dias C, Barbot C, Carrilho I, Santos M, Malik I, Gitschier J, Hayflick SJ: **Neurodegeneration associated with genetic defects in phospholipase A_2.** *Neurology* 2008, **71**:1402–1409.
2. Gregory A, Polster BJ, Hayflick SJ: **Clinical and genetic delineation of neurodegeneration with brain iron accumulation.** *J Med Genet* 2009, **46**:73–80.
3. Seitelberger F: **Neuroaxonal dystrophy: its relation to aging and neurological diseases.** In *Handbook of Clinical Neurology. Volume 5.* Edited by Vinken PJ, Bruyn GW, Klawans HL. Amsterdam: Elsevier; 1986:391–415.
4. Kurian MA, Morgan NV, MacPherson L, Foster K, Peake D, Gupta R, Philip SG, Hendriksz C, Morton JEV, Kingston HM, Rosser EM, Wassmer E, Gissen P, Maher ER: **Phenotypic spectrum of neurodegeneration associated with mutations in the PLA2G6 gene (PLAN).** *Neurology* 2009, **70**:1623–1629.
5. Morgan NV, Westaway SK, Morton JE, Gregory A, Gissen P, Sonek S, Cangul H, Coryell J, Canham N, Nardocci N, Zorzi G, Pasha S, Rodriguez D, Desguerre I, Mubaidin A, Bertini E, Trembath RC, Simonati A, Schanen C, Johnson CA, Levinson B, Woods CG, Wilmot B, Kramer P, Gitschier J, Maher ER, Hayflick SJ: **PLA2G6, encoding a phospholipase A_2, is mutated in neurodegenerative disorders with high brain iron.** *Nat Genet* 2006, **38**:752–754.
6. Wu Y, Jiang Y, Gao Z, Wang J, Yuan Y, Xiong H, Chang X, Bao X, Zhang Y, Xiao J, Wu X: **Clinical study and PLA2G6 mutation screening analysis in Chinese patients with infantile neuroaxonal dystrophy.** *Eur J Neurol* 2009, **16**:240–245.
7. Nardocci N, Zorzi G, Farina L, Binelli S, Scaioli W, Ciano C, Verga L, Angelini L, Savoiardo M, Bugiani O: **Infantile neuroaxonal dystrophy: Clinical spectrum and diagnostic criteria.** *Neurology* 1999, **52**:1472–1478.
8. Paisan-Ruitz C, Li A, Schneider SA, Holton JL, Johnson R, Kidd D, Chataway J, Bhatia KP, Lees AJ, Hardy J, Revesz T, Houlden H: **Widespread Lewy body and tau accumulation in childhood and adult onset dystonia-parkinsonism cases with PLA2G6 mutations.** *Neurobiol Aging* 2012, **33**:814–823.
9. Yoshino H, Tomiyama H, Tachibana N, Yoshino H, Tomiyama H, Tachibana N, Ogaki K, Li Y, Funayama M, Hashimoto T, Takashima S, Hattori N: **Phenotypic spectrum of patients with PLA2G6 mutation and PARK14-linked parkinsonism.** *Neurology* 2010, **75**:1356–1361.
10. Ikeuchi T, Kakita A, Shiga A, Kasuga K, Kaneko H, Tan CF, Idezuka J, Wakabayashi K, Onodera O, Iwatsubo T, Nishizawa M, Takahashi H, Ishikawa A: **Homozygous and heterozygous patients for *SNCA* duplication in family with parkinsonism and dementia.** *Arch Neurol* 2008, **65**:514–519.
11. Kaneko H, Kakita A, Kasuga K, Nozaki H, Ishikawa A, Miyashita A, Kuwano R, Ito G, Iwatsubo T, Takahashi H, Nishizawa M, Onodera O, Sisodia SS, Ikeuchi T: **Enhanced accumulation of phosphorylated α-synuclein and elevated Aβ42/40 ratio caused by expression of the presenilin-1 delta T440 mutant associated with familial Lewy body disease and variant Alzheimer disease.** *J Neurosci* 2007, **28**:13092–13097.
12. Fujiwara H, Hasegawa M, Dohmae N, Kawashima A, Masliah E, Goldberg MS, Shen J, Takio K, Iwatsubo T: **α-synuclein is phosphorylated in synucleinopathy lesions.** *Nat Cell Biol* 2002, **4**:160–164.
13. Braak H, Del Tredici K, Rüb U, de Vos RA, Jansen Steur EN, Braak E: **Staging of brain pathology related to sporadic Parkinson's disease.** *Neurobiol Aging* 2003, **24**:197–211.
14. McKeith IG, Dickson DW, Lowe J, Emre M, O'Brien JT, Feldman H, Cummings J, Duda JE, Lippa C, Perry EK, Aarsland D, Arai H, Ballard CG, Boeve B, Burn DJ, Costa D, Del Ser T, Dubois B, Galasko D, Gauthier S, Goetz CG, Gomez-Tortosa E, Halliday G, Hansen LA, Hardy J, Iwatsubo T, Kalaria RN, Kaufer D, Kenny RA, Korczyn A, Kosaka K, Lee VM, Lees A, Litvan I, Londos E, Lopez OL, Minoshima S, Mizuno Y, Molina JA, Mukaetova-Ladinska EB, Pasquier F, Perry RH, Schulz JB, Trojanowski JQ, Yamada M: **Diagnosis and management of dementia with Lewy bodies: third report of the DLB Consortium.** *Neurology* 2005, **65**:1863–1872.
15. Braak H, Alafuzoff I, Arzberger T, Kretzschmar H, Tredici KD: **Staging of Alzheimer's disease-associated neurofibrillary pathology using paraffin sections and immunocytochemistry.** *Acta Neuropathol* 2006, **112**:389–404.
16. Kosaka K: **Lewy bodies in cerebral cortex, report of three cases.** *Acta Neuropathol (Berl)* 1978, **42**:127–134.
17. Ma Z, Wang X, Nowatzke W, Ramanadham S, Turk J: **Human pancreatic islets express mRNA species encoding two distinct catalytically active isoforms of group VI phopholipase A2 (iPLA2) that arise from an exon-skipping mechanism of alternative splicing of the transcript from the iPLA2 gene on chromosome 22q13.1.** *J Biol Chem* 1999, **274**:9607–9616.
18. Tonelli A, Romaniello R, Grasso R, Cavallini A, Righini A, Bresolin N, Borgatti R, Bassi MT: **Novel splice-site mutations and a large intragenic deletion in PLA2G6 associated with a severe and rapidly progressive form of infantile neuroaxonal dystrophy.** *Clin Genet* 2010, **78**:432–440.
19. Li A, Paudel R, Johnson R, Courtney R, Lees AJ, Holton JL, Hardy J, Revesz T, Houlden H: **Pantothenate kinase-associated neurodegeneration is not a synucleinopathy.** *Neuropathol Appl Neurobiol* 2013, **39**:121. 131.
20. Wakabayashi K, Fukushima T, Koide R, Horikawa Y, Hasegawa M, Watanabe Y, Noda T, Eguchi I, Morita T, Yoshimoto M, Iwatsubo T, Takahashi H: **Juvenile-onset generalized neuroaxonal dystrophy (Hallervorden-Spatz disease) with diffuse neurofibrillary and Lewy body pathology.** *Acta Neuropathol (Berl)* 2000, **99**:331–336.
21. Wakabayashi K, Yoshimoto M, Fukushima T, Koide R, Horikawa Y, Morita T, Takahashi H: **Widespread occurrence of α-synuclein/NACP immunoreactive neuronal inclusions in juvenile and adult-onset Hallervorden–Spatz disease with Lewy bodies.** *Neuropathol Appl Neurobiol* 1999, **25**:363–368.
22. Neumann M, Adler S, Schlüter O, Kremmer E, Benecke R, Kretzschmar HA: **α-Synuclein accumulation in a case of neurodegeneration with brain iron accumulation type 1 (NBIA-1, formerly Hallervorden-Spatz syndrome) with wide spread cortical and brainstem-type Lewy bodies.** *Acta Neuropathol (Berl)* 2000, **100**:568–574.

23. Forno LS: **Neuropathology of Parkinson's disease.** *J Neuropathol Exp Neurol* 1996, **55**:259–272.
24. Hawkes CH, Tredici KD, Braak H: **Review: Parkinson's disease: a dual-hit hypothesis.** *Neuropathol Appl Neurobiol* 2007, **33**:599–614.
25. Orimo S, Takahashi A, Uchihara T, Mori F, Kakita A, Wakabayashi K, Takahashi H: **Degeneration of cardiac sympathetic nerve begins in the early disease process of Parkinson's disease.** *Brain Pathol* 2007, **17**:24–30.
26. Iseki E, Marui W, Kosaka K: **Frequent coexistence of Lewy bodies and neurofibrillary tangles in the same neurons of patients with diffuse Lewy body disease.** *Neurosci Lett* 1999, **265**:9–12.
27. Ishizawa T, Mattila P, Davies P, Wang D, Dickson DW: **Colocalization of tau and alpha-synuclein epitopes in Lewy bodies.** *J Neuropathol Exp Neurol* 2003, **62**:389–397.
28. Baburina I, Jakowski S: **Cellular responses to excess phospholipid.** *J Biol Chem* 1999, **14**:9400–9408.
29. Beck G, Sugiura Y, Shinzawa K, Kato S, Setou M, Tsujimoto Y, Sakoda S, Sumi-Akamaru H: **Neuroaxonal dystrophy in calcium-independent phospholipase $A_2\beta$ deficiency results from insufficient remodeling and degeneration of mitochondrial and presynaptic membranes.** *J Neurosci* 2011, **31**:11411–11420.
30. Malik I, Turk J, Mancuso DJ, Montier L, Wohltmann M, Wozniak DF, Schmidt RE, Gross RW, Kotzbauer PT: **Disrupted membrane homeostasis and accumulation of ubiquitinated proteins in a mouse model of infantile neuroaxonal dystrophy caused by PLA2G6 mutations.** *Am J Pathol* 2008, **172**:406–416.
31. Shinzawa K, Sumi H, Ikawa M, Matsuoka Y, Okabe M, Sakoda S, Tsujimoto Y: **Neuroaxonal dystrophy caused by group VIA phospholipase A_2 deficiency in mice: a model of human neurodegenerative disease.** *J Neurosci* 2008, **28**:2212–2220.
32. Wada H, Yasuda T, Miura I, Watabe K, Sawa C, Kamijuku H, Kojo S, Taniguchi M, Nishino I, Wakana S, Yoshida H, Seino K: **Establishment of an improved mouse model for infantile neuroaxonal dystrophy that shows early disease onset and bears a point mutation in Pla2g6.** *Am J Pathol* 2009, **175**:2257–2263.
33. Hamilton RL: **Lewy bodies in Alzheimer's disease: A neuropathological review of 145 cases using α-synuclein immunohistochemistry.** *Brain Pathol* 2000, **10**:378–384.
34. Rosenberg CK, Pericak-Vance MA, Saunders AM, Gilbert JR, Gaskell PC, Hulette CM: **Lewy body and Alzheimer pathology in a family with the amyloid-β precursor protein APP717 gene mutation.** *Acta Neuropathol (Berl)* 2000, **100**:145–152.
35. Saito Y, Ruberu NN, Sawabe M, Arai T, Kazama H, Hosoi T, Yamanouchi H, Murayama S: **Lewy body-related α-synucleinopathy in aging.** *J Neuropathol Exp Neurol* 2004, **63**:742–749.
36. Saito Y, Suzuki K, Hulette CM, Murayama S: **Aberrant phosphorylation of α-synuclein in human Niemann-Pick type C1 disease.** *J Neuropathol Exp Neurol* 2004, **63**:323–328.

doi:10.1186/2051-5960-1-12
Cite this article as: Riku *et al.*: Extensive aggregation of α-synuclein and tau in juvenile-onset neuroaxonal dystrophy: an autopsied individual with a novel mutation in the *PLA2G6* gene-splicing site. *Acta Neuropathologica Communications* 2013 **1**:12.

Ann Allergy Asthma Immunol 112 (2014) 23–28

Contents lists available at ScienceDirect

Interleukin-18 expression, CD8$^+$ T cells, and eosinophils in lungs of nonsmokers with fatal asthma

Hanako Oda, MD [*]; Tomotaka Kawayama, MD [*]; Haruki Imaoka, MD [*]; Yuki Sakazaki, MD [*]; Yoichiro Kaku, MD [*]; Masaki Okamoto, MD [*]; Yasuhiko Kitasato, MD [*]; Nobutaka Edakuni, MD [*]; Shin-ichi Takenaka, MD [*]; Makoto Yoshida, MD [†]; Tomoaki Iwanaga, MD [†]; Seiya Kato, MD [‡]; Paul M. O'Byrne, MD [§]; and Tomoaki Hoshino, MD [*]

[*] *Division of Respirology, Neurology, and Rheumatology, Department of Medicine 1, Kurume University School of Medicine, Kurume, Japan*
[†] *Fukuoka National Hospital, Fukuoka, Japan*
[‡] *Division of Pathology and Cell Biology, Graduate School and Faculty of Medicine, University of the Ryukyus, Okinawa, Japan*
[§] *Department of Medicine, McMaster University, Hamilton, Ontario, Canada*

ARTICLE INFO

Article history:
Received for publication July 16, 2013.
Received in revised form August 26, 2013.
Accepted for publication September 1, 2013.

ABSTRACT

Background: The process of airway inflammation in the lungs of nonsmokers who die of asthma (fatal asthma) has not been reported in detail.
Objective: To examine nonsmokers who had died of asthma to exclude chronic obstructive pulmonary disease and investigate pulmonary inflammatory cells and the expression of interleukin-18 (IL-18) and its receptor in lung tissues compared with those in patients with well-controlled mild asthma and nonsmokers.
Methods: Lung tissues were obtained at autopsy examination from 12 nonsmokers with fatal asthma, excluding cases of chronic obstructive pulmonary disease, and from 5 nonsmokers with well-controlled mild asthma and 10 nonsmokers who had undergone surgical resection for lung cancer. Pulmonary inflammatory cells were examined and the expression of the proinflammatory cytokine IL-18 and its receptor in the lungs was evaluated.
Results: The numbers of eosinophils and lymphocytes, but not basophils or macrophages, were significantly increased in the lungs of patients with fatal asthma compared with the other 2 groups. The lung neutrophil count did not differ significantly between the fatal and mild asthma groups but was significantly higher in the fatal asthma group than in nonsmokers. CD8$^+$ T cells, but not CD4$^+$ T cells, were significantly increased in the lungs of the fatal asthma group compared with the other 2 groups. IL-18 protein and IL-18 receptor were strongly expressed in the lungs in the fatal asthma group.
Conclusion: Caspase-1 inhibitors, anti–IL-18 antibodies, anti–IL-18 receptor antibodies, IL-18 binding protein, or inhibitors of genes downstream of the IL-18 signal transduction pathway may be of clinical benefit for the treatment of patients with severe asthma.

Introduction

Autopsy studies of the lungs of patients with fatal asthma, conducted in the 1950s, reported that the outstanding feature was the presence of numerous mucus plugs in the airways and focal areas of collapse.[1,2] Thereafter, several series of studies of fatal asthma cases reported the presence of severe airway remodeling accompanied by mucus plugging, goblet cell hyperplasia, smooth muscle hypertrophy, submucosal gland hyperplasia, basement membrane thickening, and eosinophilic inflammation.[3–7] In addition, severe airway remodeling was found in the large and small airways of patients who had died of asthma.[8–10] These results suggested that severe airway remodeling and pulmonary inflammatory cells might be involved in the pathogenesis of death from asthma.[11]

Studies of bronchial biopsies have shown that nonsmokers with mild and stable asthma have increased numbers of activated CD4$^+$ T cells producing T-helper cell type 2 [T_H2] cytokines (eg, interleukin [IL]-4, IL-5, and IL-13) and eosinophils in the mucosa of the large airways. A previous study reported that CD8$^+$ T cells were

Reprints: Tomoaki Hoshino, MD, Division of Respirology, Neurology and Rheumatology, Department of Medicine 1, Kurume University School of Medicine, 67 Asahi-machi, Kurume 830-0011, Japan; E-mail: hoshino@med.kurume-u.ac.jp.
Disclosures: Authors have nothing to disclose.
Funding Sources: This work was supported by a grant to the Respiratory Failure Research Group from the Ministry of Health, Labor and Welfare, Japan; a Grant-in-Aid for Scientific Research (21590977 to Dr Hishino) from the Ministry of Education, Science, Sports, and Culture of Japan; the Kato Memorial Fund for Incurable Diseases Research (Tokyo, Japan; to Dr Hoshino); the Kaibara Morikazu Medical Science Promotion Foundation (to Dr Imaoka); the Allergy Foundation (to Dr Imaoka); and the Takeda Science Foundation (to Dr Imaoka).

1081-1206/13/$36.00 - see front matter
http://dx.doi.org/10.1016/j.anai.2013.09.004

increased in the airways in some fatal cases of asthma.[12] Moreover, $CD8^+$ T cells producing the T-helper cell type 1 [T_H1] cytokine interferon-γ (IFN-γ) are reportedly increased in the lungs of patients with severe asthma, including fatal asthma.[13] However, it is still unclear whether $CD8^+$ T cells and/or $CD4^+$ T cells are involved in the pathogenesis of asthma deaths. It is noteworthy that the patients analyzed in the previous studies included smokers, ex-smokers, or patients with asthma whose smoking status was unknown.[14] Moreover, in the 1950s, it was believed that the major pathologic findings of fatal asthma was plugging of the bronchial tree with mucus, eosinophilia, thickening of the basement membrane, and emphysema.[1] Therefore, some of those patients[14] and those studied in the 1940s and 1950s[1] may have had chronic obstructive pulmonary disease (COPD) with or without asthma.

Interleuin-18 is a proinflammatory cytokine, originally discovered as an IFN-γ–inducing factor. IL-18 is a member of the IL-1 family of cytokines.[15] Like IL-1, IL-33, IL-36, IL-37, and IL-38, IL-18 is produced intracellularly from a biologically inactivated precursor, pro–IL-18. Mature IL-18 is secreted after cleavage of pro–IL-18 by caspase-1, originally identified as an IL-1β converting enzyme. Activated macrophages produce large amounts of mature IL-18 after cleavage of pro–IL-18 by caspase-1.[16] IL-18 plays a well-known important role in T_H1 polarization and can act as a cofactor for T_H2 cell development and IgE production.[16–19] It also plays important roles in the pathogenesis of inflammatory and allergic diseases, such as rheumatoid arthritis, adult-onset Still disease, Sjögren syndrome, inflammatory bowel diseases including Crohn disease, allergic rhinitis, and atopic dermatitis.[16,20,21] IL-18 also is involved in the development of lung diseases, including lung injury,[22,23] idiopathic pulmonary fibrosis,[24] and COPD.[25] Recently, the authors reported that IL-18 protein was strongly expressed in airway epithelial and smooth muscle cells in airway biopsy samples from patients with allergic asthma. Moreover, the serum levels of IL-18 were significantly higher in patients with asthma than in patients without asthma with allergy or healthy controls.[26] The present study selected 12 nonsmokers who had died of asthma and excluded any with COPD and investigated pulmonary inflammatory cells and the expression of IL-18 and its receptor (IL-18R) in their lung tissues compared with controls.

Methods

Patients

This study carefully excluded smokers and ex-smokers and analyzed nonsmokers to exclude any with COPD. Twelve patients (9 male and 3 female, 5–79 years old) diagnosed as having asthma were monitored at Kurume University Hospital (Kurume, Japan) and the Fukuoka National Hospital (Fukuoka, Japan). These patients with asthma were nonsmokers and had died from 1973 to 1998. Lung tissues were obtained at autopsy examination in each case. The details of these 12 patients are listed in Table 1. As materials for comparison, lung tissues were obtained from 5 nonsmokers with mild asthma (1 male and 4 female, 58–79 years old) and normal lung tissues were obtained as controls from 10 nonsmokers (5 male and 5 female, 27–78 years old), all of whom underwent surgical resection for lung cancer at Kurume University Hospital (Table 2). Sample collection and all procedures were approved by the ethics committees of Kurume University in accordance with the ethical standards of the Declaration of Helsinki of 1975.

Pulmonary Function Tests

Japanese predicted normal values were used to calculate the predicted percentage of forced expiratory volume in 1 second, which met the Japanese Pulmonary Function Standard in the Japanese Respiratory Society Statement, as previously reported.[27] Further details of these analyses are provided in the online supplementary data.

Histology

Lung tissues were fixed with 10% formalin and embedded in paraffin wax, as reported previously.[24] One to 3 paraffin-embedded lung tissues were obtained from each patient. Sequential sections were made from each paraffin-embedded lung tissue. Sections (4 μm thick) were serially cut, placed on poly-L-lysine–coated slides, and incubated overnight at 55°C to 60°C. Deparaffinized sections were stained with hematoxylin and eosin and May-Giemsa stain. Then, digitized video images of the entire lung fields were captured by a CCD camera and were modulated by Adobe Photoshop CS (Adobe, Tokyo, Japan), as previously reported.[24,25]

Quantitative Assessment of Infiltrating Inflammatory Cells in Lung Tissues

Pulmonary inflammatory cells, such as eosinophils, basophils, neutrophils, lymphocytes, and alveolar macrophages, were counted. Briefly, in May-Giemsa–stained sections of lung tissues, 3 square fields at ×40 magnification (2.5 × 3.5 mm, 8.75 mm^2) were selected in which small-airway inflammation appeared most severe; within each field, 4 other individual square fields at ×400 magnification (0.22 × 0.32 mm, 0.0704 mm^2) were selected. These smaller square fields were defined as observation fields (OFs), and 12 different OFs were selected within 3 different square fields (3 × 8.75 mm^2) on each lung section. Eosinophils, basophils, neutrophils, lymphocytes, and alveolar macrophages were

Table 1
Characteristics of 12 nonsmokers with fatal asthma

Patient number	Age	Sex	Year of autopsy examination	Therapy						Duration from asthma attack
				Systemic corticosteroid	ICS	β_2 Agonist	Theophylline	Leukotriene receptor antagonist	Ventilator	
1	32	M	1973	+	−	−	+	−	−	75 min
2	52	M	1974	+	−	−	−	−	−	5 d
3	5	M	1977	−	−	−	−	−	+	36 h
4	67	M	1980	−	−	−	−	−	−	5 h
5	44	M	1981	+	−	−	−	−	−	<24 h
6	75	M	1982	+	−	−	−	−	−	20 min
7	16	F	1984	−	−	+	+	−	−	DOA (6 h)
8	79	F	1986	+	−	−	−	−	+	6 d
9	57	M	1986	+	−	−	−	−	−	unknown
10	14	M	1994	−	−	−	−	−	−	DOA (13 d)
11	24	M	1998	+	+	+	+	−	−	4 d
12	68	F	1998	−	+	−	−	−	+	DOA (7 d)

Abbreviations: DOA, death on arrival; F, female; ICS, inhaled corticosteroid; M, male.

Table 2
Characteristics of patients with fatal asthma, those with mild asthma, and control patients

	Asthma death	Mild asthma	Control
Patients (male/female), n	12 (9/3)	5 (1/4)	10 (5/5)
Age (y), mean ± SD	44.4 ± 7.4	66.8 ± 4.1	62.5 ± 4.9
Body mass index (kg/m^2), mean ± SD	20.61 ± 1.0	25.0 ± 1.9	22.9 ± 1.8
FVC (% predicted), mean ± SD	ND	107.5 ± 6.7	107.3 ± 7.8
FEV_1 (% predicted), mean ± SD	ND	97.3 ± 11.0	103.3 ± 7.0
FEV_1/FVC (%), mean ± SD	ND	66.2 ± 6.51	78.9 ± 2.8
WBC count (cells/μL), mean ± SD	ND	6233 ± 521	5530 ± 576
Eosinophils (cells/μL), mean ± SD	ND	168 ± 83[a]	90 ± 11

Abbreviations: FEV_1, forced expiration in 1 second; FVC, forced vital capacity; ND, not done; SD, standard deviation; WBC, white blood cell.
[a] $P < .05$ vs control patients.

counted within each of the 12 OFs. Results were expressed as mean ± standard error of the mean for cells per square millimeter. For example, when 20 lymphocytes were counted within 1 OF at ×400 magnification, the number of lymphocytes was 284 cells/mm^2. Two examiners manually counted these lung sections independently and in a blinded manner, without prior knowledge of the patients' clinical status.

Immunohistochemical Assay

Immunohistochemical analysis was performed as reported previously.[23–25] Antihuman CD4 monoclonal antibody (mAb; 4B12 [mouse IgG1]; Dako, Tokyo, Japan), antihuman CD8 mAb (C8/144B [mouse IgG1]; Dako), antihuman IL-18 mAb (1-8D [mouse IgG1][23] or clone 8 [mouse IgG2a],[24] kindly provided by Dr Do-Young Yoon, Laboratory of Cellular Biology, Korea Research Institute of Bioscience and Biotechnology, Taejon, Korea), and anti–IL-18R α-chain (IL-18Rα; H44 [mouse IgG1])[24] were applied to the sections at 4°C for 18 hours. Positive reactivity was identified by Permanent Red (Dako) using an EnVision G|2 System/AP (Dako) with rabbit/mouse (Permanent Red) or 3-3′-diaminobenzidine-4HCl (DAB) using an EnVision+ kit with horseradish peroxidase (Dako). Further details of these analyses are provided in the eMethods.

Statistical Analysis

Results are expressed as mean ± standard error of the mean. Nonparametric tests (Kruskal-Wallis test and Mann-Whitney *U* test) were used to compare differences among groups. SAS 9.1.3 (Japanese edition; SAS Institute, Cary, North Carolina) was used for statistical analysis. A *P* value less than .05 was considered statistically significant.

Results

Clinical Findings

All 12 patients with fatal asthma were nonsmokers, and none had COPD. Their ages ranged from 5 to 79 years (mean age 44.4 years). Five of the 12 patients had died within 24 hours after the onset of the asthma attack. The duration of disease in these patients with asthma covered a wide range, from 10 months to 50 years; 9 patients had had asthma for longer than 6 years. Seven patients had been treated with systemic corticosteroid, and only 2 had been receiving inhaled corticosteroid (ICS; beclomethasone dipropionate). The other 10 patients had died without treatment with systemic corticosteroid or ICS (Table 1). Lung tissues also were obtained from 5 nonsmokers with mild asthma and 10 nonsmokers, all of whom had undergone surgical resection for lung cancer. The 5 patients with mild asthma showed a significantly decreased ratio of the percentage of forced expiratory volume in 1 second to forced vital capacity and a significant increase of the peripheral eosinophil count compared with the control patients (Table 2). Three patients with mild asthma had been treated with ICS at the time of surgery: 2 had received 400 μg of fluticasone propionate and 1 had received 400 μg of fluticasone propionate. Another 2 patients with mild asthma had not received any form of medication.

Histopathologic Characteristics of the Lungs in Fatal Cases of Asthma

Representative examples of the histology of the lung tissues obtained from 2 patients with fatal asthma are shown in Figure 1A. Hematoxylin and eosin staining showed severe airway remodeling, and pulmonary inflammation was evident in the lung tissues obtained from 2 men who had been 32 and 52 years old (patients 1 and 2 in Table 1). Severe airway remodeling accompanied by hypertrophy of smooth muscle, airway wall edema, hyperplasia and hypertrophy of goblet cells, mucous plugs, and massive pulmonary inflammation were observed in all 12 patients with fatal asthma, including a 5-year-old boy (patient 3). Emphysematous change was not observed in the lungs of any of the 12 patients with fatal asthma. In contrast to the fatal asthma group, airway remodeling was barely evident in the lung tissues obtained from the 5 patients with mild asthma and the 10 nonsmokers, as reported previously (data not shown).[26]

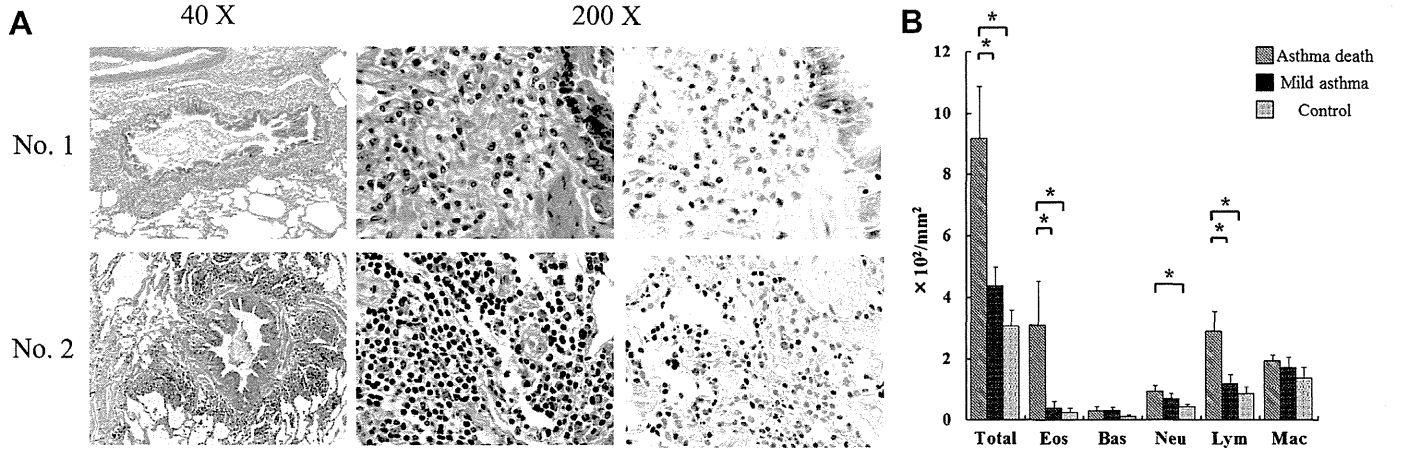

Figure 1. Histologic analysis of lungs obtained from patients who died of asthma. *(A)* Hematoxylin and eosin (×40 and ×200) and May-Giemsa staining of lung tissue samples (×200). *(B)* Quantitative analysis showed that counts of eosinophils (Eos) and lymphocytes (Lym) were significantly larger in the airways of patients who died of asthma (n = 12) than in those of patients with mild asthma (n = 5) or controls (n = 10). *$P < .05$. Bas, basophils; Mac, macrophages; Neu, neutrophils.

Examination of May-Giemsa–stained lung sections from the fatal asthma group showed massive accumulation of eosinophils and lymphocytes in the airways, especially the submucosa and basal membrane, whereas basophils, alveolar macrophages, and neutrophils were scarcely evident (*right panels* in Fig 1A). Quantitative analysis showed that the airway counts of total cells, namely eosinophils and lymphocytes, but not alveolar macrophages or basophils, were significantly ($P < .05$) higher in the fatal asthma group than in the mild asthma or control group. Neutrophils were not increased significantly in the fatal asthma group compared with the mild asthma group, although the neutrophil count was significantly larger in the former group than in the control group (Fig 1B).

Increase of CD8$^+$ T Cells in Airways of Patients with Fatal Asthma

Because lymphocytes were greatly increased in the lungs of patients with fatal asthma, the authors investigated which T-cell population was increased in this group. Sequential sections were prepared from paraffin-embedded lung tissues obtained from all 3 groups of patients and subjected to immunohistochemical analysis using anti-CD4 and anti-CD8 mAbs. This showed the presence of CD4$^+$ T cells in the lungs of the fatal asthma group, and CD8$^+$ T cells were especially increased in the airways of this group. Figure 2A shows representative examples of immunohistochemical analysis of CD4$^+$ T cells and CD8$^+$ T cells in the lungs obtained from a 16-year-old girl (patient 7). Quantitative analysis showed that the counts of CD4$^+$ T cells in the lungs of the fatal asthma group, mild asthma group, and control group were 65.9 ± 11.5, 49.0 ± 10.0, and 14.8 ± 2.9 cells/mm^2, respectively. CD4$^+$ T cells were significantly ($P < .05$) more numerous in the lungs in the fatal asthma and mild asthma groups than in the control group; the difference between the former 2 groups was not significant. The counts of CD8$^+$ T cells in the airways of the 3 groups were 170.9 ± 25.2, 73.5 ± 24.1, and 54.5 ± 14.1 cells/mm^2, respectively, being significantly ($P < .05$) increased in the fatal asthma group, but not in the other 2 groups. Moreover, the count of CD8$^+$ T cells was significantly ($P < .005$) larger than that of CD4$^+$ T cells in the lungs of patients who had died of asthma (Fig 2B).

Expression of IL-18 and IL-18Rα in the Lungs of Patients with Fatal Asthma

We examined whether IL-18 protein was expressed in the lungs of patients who had died of asthma. As reported previously,[24,25] IL-18 was expressed constitutively, but weakly, in the bronchoalveolar epithelium, alveolar macrophages, and endothelium of small vessels in control patients. In contrast, IL-18 protein and IL-18Rα were strongly expressed in inflammatory cells, airway epithelial cells, and smooth muscle in the lungs of patients with fatal asthma (Fig 3).

Discussion

In this study, the numbers of eosinophils and lymphocytes, but not neutrophils, were significantly increased in the lungs of patients with fatal asthma compared with patients with mild asthma and control nonsmokers. Moreover, CD8$^+$ T cells, but not CD4$^+$ T cells, were significantly increased in the lungs of the fatal asthma group compared with the other 2 groups. It has been proposed that fatal asthma can be differentiated according to the time from the onset of an acute attack to the time of death.[28,29] A previous study has shown that eosinophils exceed neutrophils in the airway submucosa of patients with slow-onset fatal asthma, whereas neutrophils exceed eosinophils in patients with sudden-onset fatal asthma.[28] In addition, patients in whom the duration of a terminal asthma attack exceeded 24 hours have been shown to have a significantly larger count of activated eosinophils than patients who died suddenly.[30] In contrast, severe asthma exacerbations from noninfective causes are characterized by increased eosinophil activation and IL-5 in sputum.[31] In the present study, 12 patients who died of asthma and were nonsmokers were examined. Five of 12 patients died within 24 hours and were classified as having sudden-onset fatal asthma. In the present study, there was no significant difference in eosinophil counts in patients with fatal asthma who died within 24 hours vs longer than 24 hours after the onset of the asthma attack (data not shown). These results suggest that eosinophils were chronically increased and/or activated in the lungs of the patients before the fatal attack. Neutrophils were not significantly increased in the fatal asthma group compared with the mild asthma group, although neutrophils were significantly increased in the former compared with the control group. Moreover, none of the patients in the fatal asthma group showed an increase in the neutrophil count compared with eosinophils or lymphocytes (data not shown). It is well known that CD8$^+$ T cells, neutrophils, eosinophils, and/or macrophages are increased in the lungs of patients with severe COPD and in those with exacerbation of COPD.[15] Moreover, viral infections

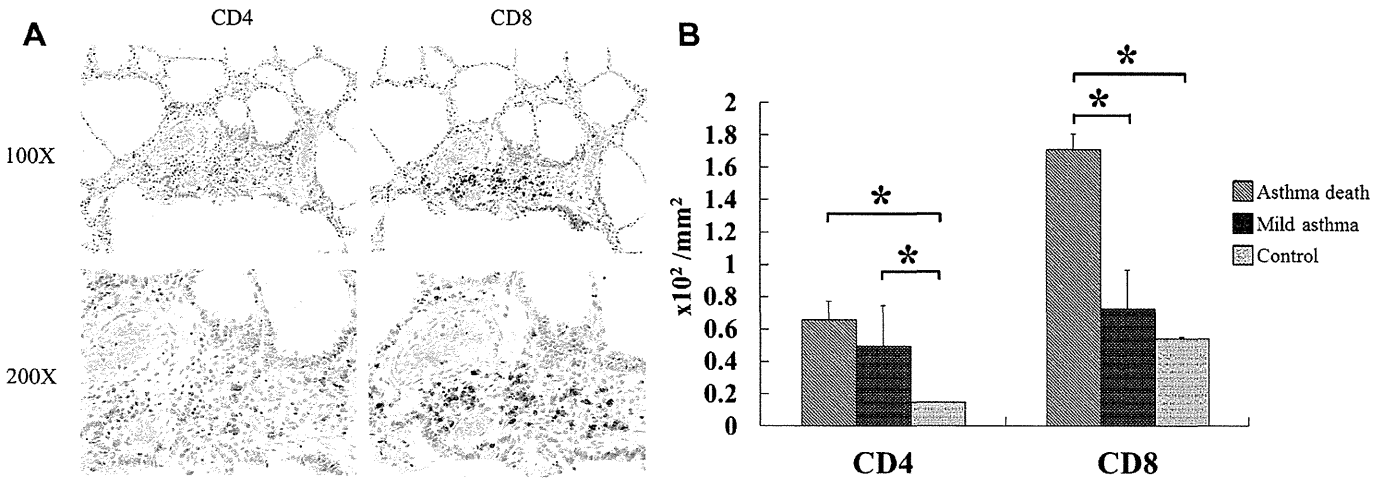

Figure 2. Immunostaining of lung tissue samples from patients who died of asthma using mouse anti-CD4 and mouse anti-CD8 monoclonal antibodies. *(A)* Positive staining for CD4 and CD8 is evident in lung tissue samples from patients who died of asthma (×100 and ×200). Positive reactivity was identified by Permanent Red (Dako). *(B)* Quantitative analysis showed that CD8$^+$ T cells were significantly increased in the airways of patients who died of asthma (n = 12), but not in those of patients with mild asthma (n = 5) or controls (n = 10). $^*P < .05$.

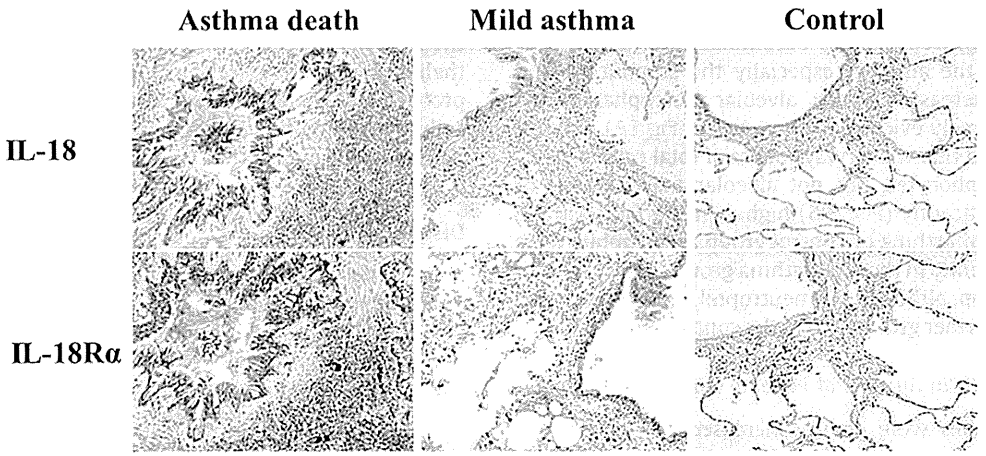

Figure 3. Immunostaining of lung tissue samples with mouse anti–interleukin-18 (IL-18) and interleukin-18 receptor α (IL-18Rα) from patients who died of asthma, patients with mild asthma, and control nonsmokers (×200). IL-18 and IL-18Rα positive reactivities were identified by 3-3′-diaminobenzidine-4HCl treatment (*brown*).

characteristically elicit strong $CD8^+$ T cells predominated by cytotoxic IFN-γ–secreting cells.[29] Therefore, the present findings suggest that previous studies may have included patients with COPD, patients with COPD and asthma, or patients with viral infection.[28,29] The present study showed that neutrophils may not be dramatically increased in the lungs of patients with sudden-onset fatal asthma or life-threatening asthma. Treatment with systemic corticosteroids was compared with nontreatment in fatal asthma. The number of neutrophils was not significantly different between the 2 groups. These results suggest that systemic corticosteroids may not affect neutrophil inflammation in the lungs of patients who succumbed to the effects of asthma.

Interleukin-18 strongly induces IFN-γ production upon exposure to various stimuli and can induce T_H2 responses.[16–19] Patients with acute asthma have higher serum IL-18 levels than normal control subjects. The IL-18 level has a tendency to correlate inversely with peak expiratory flow,[32,33] and the secretion of IL-18 from mononuclear cells of patients with bronchial asthma and atopic dermatitis is significantly higher than that in nonallergic controls.[34] It has been reported that the IL-18 gene polymorphism is significantly associated with the disease severity of asthma, with the re5744247 variant reflecting higher transcriptional activity and higher expression of IL-18 in lipopolysaccharide-stimulated monocytes and higher serum IL-18 levels.[35] IL-18R is a Toll-like receptor superfamily. Patients with fatal asthma were reported to have higher Toll-like receptor 2, 3, and 4 expression in the epithelial and airway compared with deceased control subjects.[36] Recently, the authors found that overexpression of IL-18 in the lungs can induce airway hyper-responsiveness and pulmonary inflammation through upregulating $CD4^+$ T cells and IL-13.[37] These findings suggest that IL-18 and IL-18R may be related to the severity of asthma. In the present study, the authors found that bronchoalveolar epithelial, smooth muscle, and pulmonary inflammatory cells strongly expressed IL-18 protein and IL-18Rα in the lungs of patients who died of asthma, whereas this was not the case in patients with mild asthma or normal controls. These results suggest that IL-18 released from bronchoalveolar epithelial cells and inflammatory cells, such as alveolar macrophages, can activate $CD8^+$ T cells in the airways of patients with severe asthma. Thereafter, IL-18 may induce T_H1 and T_H2 responses (eg, IL-4, IL-5, IL-13, and IFN-γ production) under conditions of severe allergic inflammation, with a potentially fatal outcome. A previous study showed that 12 younger (mean age 32 years) patients with fatal asthma who did not smoke had thicker basement membrane, airway smooth muscle, and outer wall areas in the small and large airways compared with 14 patients with fatal COPD who were longtime smokers (mean age 71 years).[38] The present study showed that severe airway remodeling accompanied by hypertrophy of smooth muscle, airway wall edema, and massive pulmonary inflammation was observed in all 12 patients with fatal asthma, including the 5-year-old boy. These data and a previous study suggest that fatal asthma produces severe airway remodeling regardless of age. It is known that the fungal allergens, especially *Alternaria alternate*, cause fatal asthma exacerbations. Sensitization and exposure to the spores of *A alternate* induce a natural helper cell-mediated rapid burst of T_H2 cytokine (IL-5 and IL-13) production and eosinophilic inflammation.[39] In this study, the authors do not know whether the allergens caused the fatal asthma exacerbations. Some patients with fatal asthma analyzed in this study may have been sensitized and challenged by *A alternate*. Further analysis is needed to test this issue.

The preferred treatment for severe persistent asthma is high-dose ICS plus a long-acting inhaled β agonist. In addition, for patients whose asthma is inadequately controlled on high-dose ICS and long-acting inhaled β agonist, a low dose of oral corticosteroids can be added. The anti-IgE humanized mAb (omalizumab) is also available. However, approximately 5% of patients with asthma are thought to have very severe disease that is resistant to high-dose ICS, oral corticosteroids, and/or anti-IgE antibody treatment. Such patients are thought to be at greatest risk of death from asthma. Therefore, new anti-inflammatory treatments are needed for severe asthma, especially asthma that is resistant to high-dose ICS and/or systemic steroid. The present study has shown the overproduction of IL-18 in the lungs of patients who succumbed to asthma. These results raise the possibility that blockade of IL-18 may be a feasible treatment for very severe asthma. Caspase-1 inhibitors, anti–IL-18 antibodies, anti–IL-18R antibodies, IL-18 binding protein, or inhibitors of genes downstream of the IL-18 signal transduction pathway, such as myeloid differentiation primary response gene 88, interleukin receptor-associated kinase, tumor necrosis factor receptor-associated factor 6, nuclear factor-κB, c-Jun N-terminal kinase, and p38 microtubule-associated protein kinase, may be of clinical benefit for the treatment of patients with severe asthma.

Acknowledgments

The authors express their sincere gratitude to the late Prof Hisamichi Aizawa (who died on February 11, 2011) for his valuable contribution to the design and conduct of the present study. They thank Dr Howard A. Young (National Cancer Institute, Frederick, Maryland) for editing and Ms Kumika Miyabaru, Ms Emiko Kuma,

Ms Chitoshi Ohki, and Ms Kyoko Yamaguchi (Kurume University) for their technical assistance.

Supplementary Data

Supplementary data related to this article can be found online at http://dx.doi.org/10.1016/j.anai.2013.09.004.

References

[1] Houston JC, De Navasquez S, Trounce JR. A clinical and pathological study of fatal cases of status asthmaticus. *Thorax*. 1953;8:207–213.

[2] Cardell BS. Pathological findings in deaths from asthma. *Int Arch Allergy Appl Immunol*. 1956;9:189–199.

[3] Messer JW, Peters GA, Bennett WA. Causes of death and pathologic findings in 304 cases of bronchial asthma. *Dis Chest*. 1960;38:616–624.

[4] Dunnill MS, Massarella GR, Anderson JA. A comparison of the quantitative anatomy of the bronchi in normal subjects, in status asthmaticus, in chronic bronchitis, and in emphysema. *Thorax*. 1969;24:176–179.

[5] Sobonya RE. Quantitative structural alterations in long-standing allergic asthma. *Am Rev Respir Dis*. 1984;130:289–292.

[6] Aikawa T, Shimura S, Sasaki H, et al. Marked goblet cell hyperplasia with mucus accumulation in the airways of patients who died of severe acute asthma attack. *Chest*. 1992;101:916–921.

[7] Synek M, Beasley R, Frew AJ, et al. Cellular infiltration of the airways in asthma of varying severity. *Am J Respir Crit Care Med*. 1996;154:224–230.

[8] James AL, Pare PD, Hogg JC. The mechanics of airway narrowing in asthma. *Am Rev Respir Dis*. 1989;139:242–246.

[9] Saetta M, Di Stefano A, Rosina C, et al. Quantitative structural analysis of peripheral airways and arteries in sudden fatal asthma. *Am Rev Respir Dis*. 1991;143:138–143.

[10] Carroll N, Elliot J, Morton A, et al. The structure of large and small airways in nonfatal and fatal asthma. *Am Rev Respir Dis*. 1993;147:405–410.

[11] Jeffery PK. Remodeling and inflammation of bronchi in asthma and chronic obstructive pulmonary disease. *Proc Am Thorac Soc*. 2004;1:176–183.

[12] Faul JL, Tormey VJ, Leonard C, et al. Lung immunopathology in cases of sudden asthma death. *Eur Respir J*. 1997;10:301–307.

[13] O'Sullivan S, Cormican L, Faul JL, et al. Activated, cytotoxic CD8(+) T lymphocytes contribute to the pathology of asthma death. *Am J Respir Crit Care Med*. 2001;164:560–564.

[14] Anthonisen NR, Wright EC, Hodgkin JE. Prognosis in chronic obstructive pulmonary disease. *Am Rev Respir Dis*. 1986;133:14–20.

[15] Kawayama T, Okamoto M, Imaoka H, et al. Interleukin-18 in pulmonary inflammatory diseases. *J Interferon Cytokine Res*. 2012;32:443–449.

[16] Nakanishi K, Yoshimoto T, Tsutsui H, et al. Interleukin-18 regulates both th1 and th2 responses. *Annu Rev Immunol*. 2001;19:423–474.

[17] Hoshino T, Wiltrout RH, Young HA. IL-18 is a potent coinducer of IL-13 in NK and T cells: a new potential role for IL-18 in modulating the immune response. *J Immunol*. 1999;162:5070–5077.

[18] Hoshino T, Yagita H, Ortaldo JR, et al. In vivo administration of IL-18 can induce IgE production through Th2 cytokine induction and up-regulation of CD40 ligand (CD154) expression on CD4+ T cells. *Eur J Immunol*. 2000;30:1998–2006.

[19] Hoshino T, Kawase Y, Okamoto M, et al. Cutting edge: IL-18–transgenic mice: in vivo evidence of a broad role for IL-18 in modulating immune function. *J Immunol*. 2001;166:7014–7018.

[20] Kawase Y, Hoshino T, Yokota K, et al. Exacerbated and prolonged allergic and non-allergic inflammatory cutaneous reaction in mice with targeted interleukin-18 expression in the skin. *J Invest Dermatol*. 2003;121:502–509.

[21] Takei S, Hoshino T, Matsunaga K, et al. Soluble interleukin-18 receptor complex is a novel biomarker in rheumatoid arthritis. *Arthritis Res Ther*. 2011;13:R52.

[22] Okamoto M, Kato S, Oizumi K, et al. Interleukin 18 (IL-18) in synergy with IL-2 induces lethal lung injury in mice: a potential role for cytokines, chemokines, and natural killer cells in the pathogenesis of interstitial pneumonia. *Blood*. 2002;99:1289–1298.

[23] Hoshino T, Okamoto M, Sakazaki Y, et al. Role of proinflammatory cytokines IL-18 and IL-1beta in bleomycin-induced lung injury in humans and mice. *Am J Respir Cell Mol Biol*. 2009;41:661–670.

[24] Kitasato Y, Hoshino T, Okamoto M, et al. Enhanced expression of interleukin-18 and its receptor in idiopathic pulmonary fibrosis. *Am J Respir Cell Mol Biol*. 2004;31:619–625.

[25] Imaoka H, Hoshino T, Takei S, et al. Interleukin-18 production and pulmonary function in COPD. *Eur Respir J*. 2008;31:287–297.

[26] Imaoka H, Gauvreau GM, Watson RM, et al. Interleukin-18 and interleukin-18 receptor-alpha expression in allergic asthma. *Eur Respir J*. 2011;38:981–983.

[27] Toda R, Hoshino T, Kawayama T, et al. Validation of "lung age" measured by spirometry and handy electronic FEV1/FEV6 meter in pulmonary diseases. *Intern Med*. 2009;48:513–521.

[28] Sur S, Crotty TB, Kephart GM, et al. Sudden-onset fatal asthma. A distinct entity with few eosinophils and relatively more neutrophils in the airway submucosa? *Am Rev Respir Dis*. 1993;148:713–719.

[29] O'Sullivan SM. Asthma death, CD8+ T cells, and viruses. *Proc Am Thorac Soc*. 2005;2:162–165.

[30] Azzawi M, Johnston PW, Majumdar S, et al. T lymphocytes and activated eosinophils in airway mucosa in fatal asthma and cystic fibrosis. *Am Rev Respir Dis*. 1992;145:1477–1482.

[31] Wark PA, Johnston SL, Moric I, et al. Neutrophil degranulation and cell lysis is associated with clinical severity in virus-induced asthma. *Eur Respir J*. 2002;19:68–75.

[32] Wong CK, Ho CY, Ko FW, et al. Proinflammatory cytokines (IL-17, IL-6, IL-18 and IL-12) and Th cytokines (IFN-gamma, IL-4, IL-10 and IL-13) in patients with allergic asthma. *Clin Exp Immunol*. 2001;125:177–183.

[33] Tanaka H, Miyazaki N, Oashi K, et al. IL-18 might reflect disease activity in mild and moderate asthma exacerbation. *J Allergy Clin Immunol*. 2001;107:331–336.

[34] El-Mezzein RE, Matsumoto T, Nomiyama H, et al. Increased secretion of IL-18 in vitro by peripheral blood mononuclear cells of patients with bronchial asthma and atopic dermatitis. *Clin Exp Immunol*. 2001;126:193–198.

[35] Harada M, Obara K, Hirota T, et al. A functional polymorphism in IL-18 is associated with severity of bronchial asthma. *Am J Respir Crit Care Med*. 2009;180:1048–1055.

[36] Ferreira DS, Annoni R, Silva LF, et al. Toll-like receptors 2, 3 and 4 and thymic stromal lymphopoietin expression in fatal asthma. *Clin Exp Allergy*. 2012;42:1459–1471.

[37] Sawada M, Kawayama T, Imaoka H, et al. IL-18 Induces Airway Hyperresponsiveness and Pulmonary Inflammation via CD4(+) T Cell and IL-13. *PLoS One*. 2013;8:e54623.

[38] Senhorini A, Ferreira DS, Shiang C, et al. Airway dimensions in fatal asthma and fatal COPD: overlap in older patients. *Int J Chron Obstruct Pulmon Dis*. 2013;10:348–356.

[39] Doherty TA, Khorram N, Chang JE, et al. STAT6 regulates natural helper cell proliferation during lung inflammation initiated by Alternaria. *Am J Physiol Lung Cell Mol Physiol*. 2012;303:L577–L588.

eMethods

Pulmonary Function Tests

Pulmonary function tests, including measurement of vital capacity (VC), forced expiratory volume in 1 second (FEV_1), and forced VC (FVC), were performed by spirometry. To assess the reversibility of the airway obstruction in all patients with a ratio (percentage) of FEV_1 to FVC lower than 70%, the FEV_1 measurement was repeated 20 minutes after the inhalation of 200 μg of salbutamol. Japanese predicted normal values were used to calculate the percentages of predicted VC, FVC, and FEV_1; those predicted values met the Japanese Pulmonary Function Standard in the Japanese Respiratory Society Statement.[1]

Immunohistochemical Assay

Immunohistochemical analysis was performed as reported previously.[2–4] Immunohistochemical analysis for $CD4^+$ and $CD8^+$ cells was performed as follows. Slides were stripped of paraffin wax, autoclaved at 125°C for 5 minutes in 0.01 mol/L of sodium citrate buffer (pH 6.0; for CD4 mAb) or in Tris-EDTA buffer (1 mmol/L EDTA, 10 mmol/L Tris-HCl, pH9.0; for CD8 mAb), and treated with 0.3% H_2O_2 methanol for 10 minutes at room temperature. Blocking solution (Protein Block; Dako) was used at room temperature for 30 minutes. Antihuman CD4 (4B12 [mouse IgG1]; Dako) and antihuman CD8 (C8/144B [mouse IgG1]; Dako) were used at room temperature for 60 minutes. Positive reactivity was identified by Permanent Red (Dako) using an EnVision G|2 System/AP for rabbit/mouse (Permanent Red; Dako).

The immunohistochemical analysis for IL-18Rα$^+$ cells was performed as follows. Slides were stripped of paraffin wax, autoclaved at 125°C for 5 minutes in Tris-EDTA buffer (1 mmol/L EDTA, 10 mmol/L Tris-HCl, pH9.0), and treated with 0.3% H_2O_2 methanol for 10 minutes at room temperature. Blocking solution was used at room temperature for 30 minutes. Anti–IL-18Rα (H44 [mouse IgG1], 4 μg/mL) mAb was used at 4°C for 18 hours. Positive reactivity was identified by DAB using an EnVision Kit with horseradish peroxidase (Dako).

The immunohistochemical analysis for IL-18^+ cells was performed as follows. Slides were stripped of paraffin wax, autoclaved in 0.01 mol/L of sodium citrate buffer (pH 6.0; Dako REAL; Dako, Kyoto, Japan) at 125°C for 5 minutes, and treated with 0.3% H_2O_2 methanol for 10 minutes at room temperature. Then, the slides were washed 3 times with 0.05 mol/L of Tris buffered saline (pH 7.6; Dako) at room temperature. Blocking solution (Protein Block Serum-Free; Dako) was used at room temperature for 30 minutes to prevent nonspecific staining. Antihuman IL-18 (clone 8 [mouse IgG2a][2] and clone 1-8D [mouse IgG1])[5] mAbs were used at 4°C for 18 hours to detect human IL-18. Then, the slides were washed 3 times with Tris buffered saline (pH 7.6). Positive reactivity was identified by DAB using an EnVision Kit with horseradish peroxidase (Dako). As negative controls, mouse-purified IgG2a and IgG1 Abs (Caltag Laboratories, Burlingame, California) were used for immunohistochemical assay.

Quantitative Assessment of Cells Producing IL-18

Percentages of $CD4^+$ or $CD8^+$ cells were assessed as previously reported.[2] Nine different OFs (9 × 1.4 mm^2) were selected at ×100 magnification within 3 different square fields (3 × 8.75 mm^2), as described previously. The OFs were scanned under a microscope at ×400 magnification. The percentages of cells that expressed CD4 or CD8 were counted within 3 different areas on each OF at ×400 magnification. Then, the mean percentage of cells that expressed CD4 or CD8 within 9 OFs was calculated. Therefore, the mean number of $CD4^+$ or $CD8^+$ cells per square millimeter in inflammatory cells was calculated as: (total number of cells per square millimeter) × (mean percentage of cells expressing CD4 or CD8). Two pathologists examined these sections independently, without prior knowledge of the patients' clinical status and in a blinded manner.

eReferences

[1] Toda R, Hoshino T, Kawayama T, et al. Validation of "lung age" measured by spirometry and handy electronic FEV1/FEV6 meter in pulmonary diseases. *Intern Med*. 2009;48:513–521.

[2] Kitasato Y, Hoshino T, Okamoto M, et al. Enhanced expression of interleukin-18 and its receptor in idiopathic pulmonary fibrosis. *Am J Respir Cell Mol Biol*. 2004;31:619–625.

[3] Imaoka H, Hoshino T, Takei S, et al. Interleukin-18 production and pulmonary function in COPD. *Eur Respir J*. 2008;31:287–297.

[4] Imaoka H, Gauvreau GM, Watson RM, et al. Interleukin-18 and interleukin-18 receptor-alpha expression in allergic asthma. *Eur Respir J*. 2011;38:981–983.

[5] Hoshino T, Okamoto M, Sakazaki Y, et al. Role of proinflammatory cytokines IL-18 and IL-1beta in bleomycin-induced lung injury in humans and mice. *Am J Respir Cell Mol Biol*. 2009;41:661–670.

nature publishing group

Retinoic acid prevents mesenteric lymph node dendritic cells from inducing IL-13-producing inflammatory Th2 cells

A Yokota-Nakatsuma[1,2], H Takeuchi[1,2], Y Ohoka[1,2], C Kato[3], S-Y Song[2,3], T Hoshino[4], H Yagita[5], T Ohteki[2,6] and M Iwata[1,2]

The vitamin A (VA) metabolite retinoic acid (RA) affects the properties of T cells and dendritic cells (DCs). In VA-deficient mice, we observed that mesenteric lymph node (MLN)-DCs induce a distinct inflammatory T helper type 2 (Th2)-cell subset that particularly produces high levels of interleukin (IL)-13 and tumor necrosis factor-α (TNF-α). This subset expressed homing receptors for skin and inflammatory sites, and was mainly induced by $B220^-CD8\alpha^-CD11b^+CD103^-$ MLN-DCs in an IL-6- and OX40 ligand-dependent manner, whereas RA inhibited this induction. The corresponding MLN-DC subset of VA-sufficient mice induced a similar T-cell subset in the presence of RA receptor antagonists. IL-6 induced this subset differentiation from naive $CD4^+$ T cells upon activation with antibodies against CD3 and CD28. Transforming growth factor-β inhibited this induction, and reciprocally enhanced Th17 induction. Treatment with an agonistic anti-OX40 antibody and normal MLN-DCs enhanced the induction of general inflammatory Th2 cells. In VA-deficient mice, proximal colon epithelial cells produced TNF-α that may have enhanced OX40 ligand expression in MLN-DCs. The repeated oral administrations of a T cell-dependent antigen primed VA-deficient mice for IL-13-dependent strong immunoglobulin G1 (IgG1) responses and IgE responses that caused skin allergy. These results suggest that RA inhibits allergic responses to oral antigens by preventing MLN-DCs from inducing IL-13-producing inflammatory Th2 cells.

INTRODUCTION

Vitamin A (VA) and its metabolite retinoic acid (RA) play critical roles in gut immunity. VA supplementation significantly reduces the mortality of undernourished infants, largely by reducing the severity of infectious diarrhea.[1] VA or RA deficiency is also induced by fat malabsorption resulting from disorders, such as pancreatic insufficiency, cholestatic liver diseases, cystic fibrosis, sprue, or inflammatory bowel diseases, or from defective VA metabolism as observed in alcoholism.[2–4] Dendritic cells (DCs) in gut-related lymphoid organs express the key RA-generating enzyme retinal dehydrogenase 2 (RALDH2; aldehyde dehydrogenase 1A2, ALDH1A2) and thus can produce RA from retinol, the basic form of VA.[5,6] $RALDH2^+$ DCs express CD103, and these cells also exist in the lamina propria of the small intestine.[7–9] RA imprints gut-homing specificity on naive T and B cells upon activation.[5,10] Thus, VA deficiency causes the depletion or reduction of T cells and immunoglobulin A (IgA)-producing B cells from the small intestinal lamina propria. RA also regulates the functional differentiation of T cells. It suppresses T helper type 1 (Th1) differentiation both directly and indirectly, and reciprocally enhances Th2 differentiation under certain conditions.[11] Accordingly, VA deficiency reduces antibody responses to T cell-dependent antigens and T cell-independent type 2 antigens but not T cell-independent type 1 antigens such as lipopolysaccharide.[12,13] RA also enhances the transforming growth factor-β (TGF-β)-dependent generation of forkhead box P3 (Foxp3)$^+$ inducible regulatory T cells, but suppresses

[1]Laboratory of Immunology, Kagawa School of Pharmaceutical Sciences, Tokushima Bunri University, Kagawa, Japan. [2]JST, CREST, Tokyo, Japan. [3]Institute of Neuroscience, Tokushima Bunri University, Kagawa, Japan. [4]Department of Medicine, Kurume University School of Medicine, Fukuoka, Japan. [5]Department of Immunology, Juntendo University School of Medicine, Tokyo, Japan and [6]Department of Biodefense Research, Medical Research Institute, Tokyo Medical and Dental University, Tokyo, Japan. Correspondence: M Iwata (iwatam@kph.bunri-u.ac.jp)

Received 14 March 2013; accepted 12 October 2013; published online 13 November 2013. doi:10.1038/mi.2013.96